The Remote Sensing of Clouds and Precipitation from Space: A Review

GRAEME L. STEPHENS AND CHRISTIAN D. KUMMEROW

Department of Atmospheric Science, Colorado State University, Fort Collins, Colorado

(Manuscript received and in final form 19 December 2006)

ABSTRACT

This paper presents a critical review of a number of popular methods that have been developed to retrieve cloud and precipitation properties from satellite radiance measurements. The emphasis of the paper is on the retrieval uncertainties associated with these methods, as these shape future data assimilation applications, either in the form of direct radiance assimilation or assimilation of retrieved geophysical data, or even in the use of retrieved information as a source of model error characterization. It is demonstrated throughout the paper how cloud and precipitation observing systems developed around seemingly simple concepts are in fact very complex and largely underconstrained, which explains, in part, why assigning realistic errors to these properties has been so elusive in the past. Two primary sources of error that define the observing system are highlighted throughout: (i) the first source is errors associated with the identification of cloudy scenes from clear scenes and the identification of precipitation in cloudy scenes from nonprecipitating cloudy scenes. The problems of discriminating of cloud clear and cloud precipitation are illustrated using examples drawn from microwave cloud liquid water path and precipitation retrievals. (ii) The second source is errors introduced by the forward model and its related parameters. The forward model generally contains two main components: a model of the atmosphere and the cloud and precipitation structures imbedded in that atmosphere and a forward model of the radiative transfer that produces the synthetic measurement that is ultimately compared to the measurement. The vast majority of methods developed for deriving cloud and precipitation information from satellite measurements is highly sensitive to these model parameters, which merely reflects the underconstrained nature of the problem and the need for other information in deriving solutions. The cloud and precipitation retrieval examples presented in this paper are most often constructed around very unrealistic atmosphere models typically composed of just a few layers. The consequence is that the retrievals become too sensitive to the unobserved parameters of those layers and the atmosphere above and below. Clearly a better definition of the atmospheric state, and the vertical structure of clouds and precipitation, are needed to improve the information extracted from satellite observations, and it is for this reason that the combination of active and passive measurements offers much hope for improving cloud and precipitation retrievals.

1. Introduction

The clouds of Earth are fundamental to most aspects of human life. Through production of precipitation, they are essential for delivering and sustaining the supplies of freshwater upon which human life depends. Clouds further exert a principal influence on the planet's energy balance. It is in clouds that latent heat is released through the process of condensation and the formation of precipitation. This form of heat is elementary to the development and evolution of the planet's storm systems and, in turn, to the precipitation produced by these systems. Clouds further exert a profound influence on the solar and infrared radiation that enters and leaves the atmosphere. This influence is complex and not entirely understood, yet it has the potential to exert profound effects on climate and on forces that affect climate change (Stephens 2005). It is for these reasons, among others, that the need to observe the distribution and variability of the properties of clouds and precipitation has emerged as a priority in earth observations. Although most past and current observational programs unrealistically treat clouds and precipitation as separate entities, it is the contention of this paper that there is much to be gained scientifically in moving away from these artificial practices toward observing clouds and precipitation properties jointly.

Corresponding author address: Graeme L. Stephens, Department of Atmospheric Science, Colorado State University, Fort Collins, CO 80523-1371.
E-mail: stephens@atmos.colostate.edu

DOI: 10.1175/2006JAS2375.1

TABLE 1. Selected parameters that commonly define the retrieved state vector of various methods and their relation to the physical processes involved.

Method	Parameter sensed	Retrieval state parameter (x)
IR emission		
Thin clouds (split-window methods, section 4a)	Emission from cloud top and atmosphere below and cloud-top temperature	Cloud-top temperature, optical thickness, and particle size
Thick clouds	Emission from near-cloud-top temperature	Cloud-top temperature and surface rainfall
Microwave emission (oceans only)		
Cloud only (section 4b)	Vertically weighted emission by water vapor and cloud water and surface	Column water vapor and liquid water
Precipitating clouds (section 4c)	Column precipitation water	Surface precipitation
Microwave scattering (section 5b)	Column ice with weaker contributions by water vapor and liquid precipitation	Surface precipitation
High-frequency microwave scattering (section 5c)	Column ice with contributions from nonprecipitating ice and water vapor profile	Surface snow rate
Combinations of microwave scattering and emission (sections 4c, 5b)	Emission and scattering signatures from different levels in the column	1D precipitation profiles
Radar observations of clouds and precipitation (section 6d)	Profiles of reflectivity generally proportional to the sixth power of particle size; relates to water contents of hydrometeors	1D cloud water and ice contents and 1D precipitation water contents
Scattering of sunlight (section 5a)	Vertically weighted reflectivity from clouds	Cloud optical depth and particle size
Combinations of scattered sunlight and IR emission (ISCCP example)	Emission and scattering signatures from different levels in the column	Cloud-top temperature, optical depth, some indication of multiple layered clouds

Past studies that seek to characterize the distributions of key cloud and precipitation properties and determine the principal factors that govern such distributions point to the elementary importance of the synoptic-scale controls of the atmospheric circulations that shape our weather systems (Rossow and Cairns 1995). The vast range of scales that influence cloud and precipitation properties and the effects of these properties on weather and climate dictate a sampling strategy that inevitably requires the use of data collected from sensors flown on earth-orbiting satellites.

A number of methods for determining various cloud and precipitation parameters primarily using satellite spectral radiances have evolved over the years. A selection of these methods and parameters derived from them are listed in Table 1. Many of the parameters identified and the methods developed to produce them are reviewed in this paper.

Satellite data records are now long enough and methods mature enough that meaningful climatologies of some of the cloud and precipitation properties listed in Table 1 are emerging. For example, climatologies have been developed as part of international programs like the International Satellite Cloud Climatology Project (ISCCP) and the Global Precipitation Climatology Project (GPCP) coordinated under the auspices of the World Climate Research Program (WCRP). Other climatologies have also been developed, as in the example of the Pathfinder Atmospheres (PATMOS) program (e.g., Jacobowitz et al. 2003). These programs have been collecting radiance data from multiple satellite platforms for more than 20 yr, producing long-term statistics of cloud cover. ISCCP, for example, converts these radiances into a classification scheme based on cloud-top (pressure) height and cloud optical thickness (Rossow and Schiffer 1999). GPCP was established in 1986 and merges infrared and microwave satellite estimates of precipitation with rain gauge data from more than 6000 stations (Adler et al. 2003). These merged data are presented in the form of monthly mean precipitation data on a $2.5^\circ \times 2.5^\circ$ latitude–longitude grid beginning in 1979, but more recently GPCP has expanded this effort to include a 1×1 daily dataset starting in 1997.

The purpose of this paper is to (i) present a critical review of the different types of cloud and precipitation information derived from current satellite measurements, (ii) review the underlying basis for the estimation of this information, and (iii) offer insight into the nature of the uncertainties that can be attached to such products. A review of such methods and related uncertainties offers a useful first step to any application of such data, including the assimilation of data into local-scale, regional, or global models. The following two sections provide a general background for discussion of satellite observing systems and provide the context for

the rest of the paper. Section 3 provides the common framework used to critique the different methods. Sections 4 and 5 then critiques a selection of more popular cloud and precipitation methods. The intent is not to provide an exhaustive review of different methods, but rather demonstrate the common threads between the methods chosen in an effort to illustrate both the hidden complexity of what are thought to be simple methods and common sources of uncertainty. Section 6 then introduces the more complex topic of multisensor data analysis and it is suggested that the kinds of issues confronted in this section reflects the future directions of research on the remote sensing of clouds and precipitation.

2. Satellite observing systems

Understanding and quantifying the real capabilities of satellite-based cloud and precipitation observing systems is a complex task. A consequence of such complexities results in the way observing system errors are typically estimated and validated. Most often, these errors are only superficially derived, overlooking main error sources, and in some instances no error estimates are given. Validation of these errors too is a complex task and is one that generally has remained elusive. This then raises problems for many applications of the data, and especially to the problem of data assimilation, which requires not only credible errors on models but also credible errors applied to "measurements" or models of such measurements so as to balance appropriately the contributions of both in the assimilation system.

The complexity of satellite observing systems and the difficulty in estimating the associated uncertainties of the system can be broadly appreciated by reference to Fig. 1. This figure identifies the main components of the observing system transfer function that determines the relationship between a given input of the system and the desired output of the system. The transfer function connects the input signal $\mathbf{x}(\mathbf{r}, t)$ (referred to as the input state) that varies in space r and/or time t to the actual measured quantity $\mathbf{y}(\mathbf{r}, t)$ (satellite radiances for example), which are then connected to the output signal of the system $\hat{\mathbf{x}}(\mathbf{r}, t)$ (the retrieved state, which merely refers to the collection of physical parameters that define the system being observed and is the desired information to be extracted). Under ideal circumstances, this retrieved state identically reproduces the input signal. It is thus important to quantify the extent to which these two states differ from one another and understand the principal factors that define such departures. The input/output states in this paper are taken to be any cloud or precipitation parameter or collection of

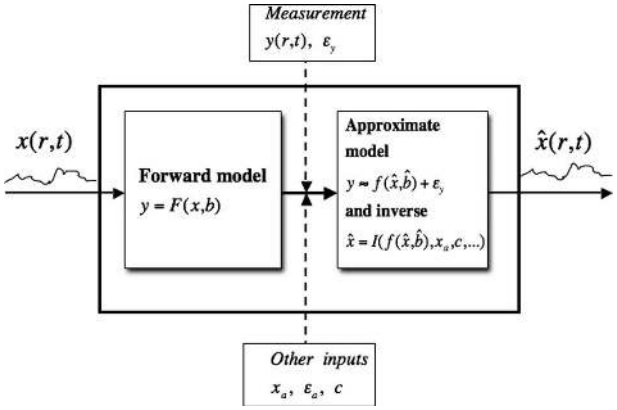

FIG. 1. A schematic of the observing system transfer function, identifying the input ($\mathbf{x}$) and output ($\hat{\mathbf{x}}$) of the system, the (physical) forward model intrinsic to the system [$F(\mathbf{x}, \mathbf{b})$], the observations and other extraneous inputs ($\mathbf{x}_a$, $\hat{\mathbf{b}}$), the approximate forward model [$f(\hat{\mathbf{x}}, \hat{\mathbf{b}})$], and its inverse $I[f(\hat{\mathbf{x}}, \hat{\mathbf{b}}), \mathbf{x}_a, \ldots]$.

parameters (as in Table 1) whose measurement over some prescribed time and space scale is the objective of the observing system.

Two basic components define the observing system transfer function. The first component has to do with the fundamental relationship between the input parameters and the measurement. This relationship is most typically established by the physical principles of radiative transfer and related processes defined by nature's forward model $F(\mathbf{x}, \mathbf{b})$ and the parameters $\mathbf{b}$ that define this "model". This part of the transfer function essentially defines the system and shapes the construction of its second component and in turn the uncertainties of the system itself. This second component refers to the entire inversion process, which begins with the relationship $f(\hat{\mathbf{x}}, \hat{\mathbf{b}})$ that approximates the forward function. The measurement $\mathbf{y}$, as well as other extraneous information, are the required inputs to this part of the system and, in combination with the approximate forward model, an "inversion" produces the output state $\hat{\mathbf{x}}$. It is in this second component of the system that several sources of uncertainty creep into the process, ultimately establishing the total system error. The various sources of error arise from the following:

(i) Measurement error (ε_y) associated with $\mathbf{y}$ due to instrument factors, including calibration uncertainties. For most satellite retrieval problems, and especially those of cloud and precipitation, this error source is usually minor compared to all others.

(ii) Forward-model error introduced by the approximate function $f(\hat{\mathbf{x}}, \hat{\mathbf{b}})$, which invariably differs from the real forward model. It is a fundamental challenge of most retrieval systems, and especially

cloud and precipitation retrieval problems, to understand and quantify such differences. This desire underscores the motivation of many model intercomparison and model development efforts, examples of which can be found in Soden et al. (2000) and Weng et al. (2007). This "forward model" approximation,

$$\mathbf{F}(\mathbf{x}, \mathbf{b}) \approx \mathbf{f}(\hat{\mathbf{x}}, \hat{\mathbf{b}}), \tag{1}$$

in most cases represents one of the most significant sources of error of the entire inversion process. This error is difficult to assess and thus is often ignored entirely.

(iii) Part of the forward-model approximation involves the replacement of key model "parameters" $\mathbf{b}$ by approximate parameters $\hat{\mathbf{b}}$. The unbiased component of the errors associated with these approximations are sometimes referred to as "geophysical noise" since they enter the inversion process in the same manner as measurement noise. These errors also often dominate retrievals, which is an indication that the retrieval problem is not properly posed and underconstrained. For cloud and precipitation retrieval problems, uncertainties associated with microphysical properties of particles (shape, size, concentrations, etc.) prevail in almost all applications and underpin many of these model parameter errors.

(iv) Errors associated with any a priori information about the "state" $\mathbf{x}_a$ that may be required to constrain the solution. Like many problems, the cloud and precipitation inverse problem is generally grossly underconstrained (e.g., Bauer et al. 2005). However, unlike more traditional sounding methods, the degree to which the problems are underconstrained tend to be less obvious, concealed by the use of overly simple forward models, the assumption of which overly influence the retrieval. A priori knowledge about the retrieved state cloud and precipitation parameters too is generally so poor that it typically offers little in way of a constraint. In many cases, retrieval problems are better formulated by shifting problematic model parameters into the retrieval state vector removing the sensitivity of the model to them. The retrieval of the backscatter-to-extinction parameter in the lidar-retrieval problem is one example (Stephens et al. 2001), as is the split-window emission method discussed in the following. Under such circumstances, a priori knowledge about such parameters plays a more substantial role in the retrieval process than is often expected.

(v) Procedures and related uncertainties required in the inversion process itself, such as convergence thresholds, among other factors. There are many ways that the actual inversion process is carried out. Some methods [e.g., cloud liquid water path (LWP) example discussed below] reduce the forward problem to such a simple form that direct inversion of the model is trivial. Other methods use forward models expressed in the form of lookup tables where inversion is achieved via interpolation of observations projected onto this table. More sophisticated inversion methods that employ more complex models typically invoke probabilistic methods like those based on the use of the Bayesian theorem often articulated in the form of variational approaches. Such approaches do not provide a single solution per se, but rather a probability distribution of solutions (the a posteriori probability) with the most probable or likely state taken to be the retrieval state. A version of this approach, popularized by Rodgers (1990, 2000) for problems dealing with sounding retrievals, is generally referred to as the optimal estimation method. Probabilistic methods have been applied in a number of cloud and precipitation retrieval problems, including the Tropical Rainfall Measuring Mission (TRMM) Goddard Profiling Algorithm (GPROF; Kummerow et al. 2001) and precipitation examples of Evans et al. (1995) or Mugnai et al. (1993), the CloudSat water content algorithm (Austin and Stephens 2001; Benedetti et al. 2003), and in the example of cloud property retrievals (Evans et al. 2002; L'Ecuyer and Stephens 2002; Cooper et al. 2003, 2007; Miller et al. 2000; among others).

Overall, the observing system is composed of the measurement and its uncertainty, an approximate forward model and related errors, including model parameters and their errors, inversion parameters and uncertainties attached to a priori knowledge. The total uncertainty of the retrieved state $\hat{\mathbf{x}}$ is the accumulation of errors from all these factors.

Yet another complicating factor arises in defining the representativeness of cloud and precipitation information derived from satellite observations. This additional complication, although not the focus of this paper, deserves mention. Representativeness errors arise, for example, when information is aggregated over space and time. These errors are primarily introduced by the space–time sampling characteristics of the observing system as imposed by the chosen orbit of the satellite platform. The effects of cloud and precipitation sampling due to sensors flown in geostationary orbit versus

low earth orbit have been studied in some detail (e.g., Salby 1982). Furthermore, the effects of the diurnal cycle on time-mean cloud and precipitation properties derived from polar-orbiting satellite observations can be found in studies like those of Salby and Callaghan (1997) and Nesbitt and Zipser (2003). An important aspect of both ISCCP and the GPCP projects is the merger of data from sensors on different satellites, both in geostationary and low earth orbit, in an effort to address these sampling issues. This is an important aspect that has to be considered when using any global datasets.

3. The physical basis of forward models

The vast majority of satellite observations of the earth's atmosphere are in the form of spectral radiances that arise as a result of natural processes of emission and scattering of electromagnetic (EM) radiation by the atmosphere and surface below. Remote sensing methods developed around such observations are referred to as passive methods, and the spectral radiances used in these methods range from the ultraviolet to the microwave regions of the EM spectrum. Unlike specific radiance measurements designed for sounding the clear atmosphere, the majority of passive methods provide very little vertical profile information about clouds and precipitation. Most of this information is in the form of (vertical) path-integrated quantities, although recent studies are beginning to suggest that some degree of cloud and precipitation vertical structure information may exist in radiance measurements (e.g., Bauer et al. 2005; Chang and Li 2005).

Given that the inherent nature of the interactions between clouds and precipitation and EM radiation vary according to the spectral region of interest, then it might be expected that the information content in such observations also varies according to where in the EM spectrum the observations are made.

Figure 2 summarizes three different classes of interactions used as the basis of forward models of satellite retrievals of cloud and precipitation properties. One class of retrieval approach relies on measurements of transmission where the attenuation of a defined source of radiation is used to determine some property of clouds. An example of this includes lidar transmission methods for thin cirrus cloud optical depth (e.g., Mitrescu and Stephens 2002) and another example is the observation of cirrus using Stratospheric Aerosol and Gas Experiment (SAGE) limb sunrise and sunset observations (Kent et al. 1993; Wang et al. 1996). A second class of method is based on information extracted from the emission of infrared and/or microwave radiation. A third method utilizes the radiation scattered by

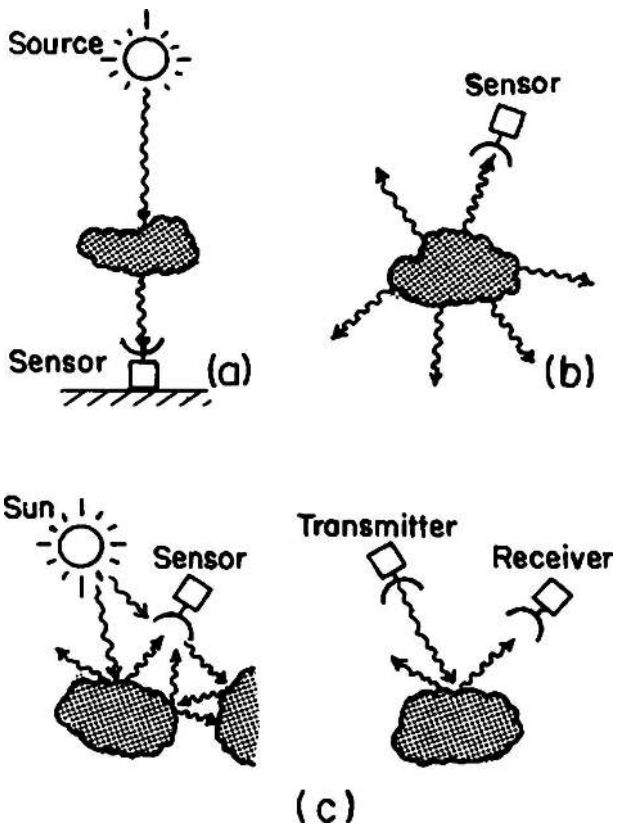

FIG. 2. A schematic of the different physical processes that establish the forward-model relationships used by different remote sensing methods applied to the study of clouds and aerosol.

clouds and precipitation. Examples of both scattering and emission methods are the topics of the following sections.

A special class of approach employs active systems, such as lidar and radar systems, for probing clouds and precipitation. Pulsed versions of such systems deliver range-resolved information about clouds and precipitation that reveals their vertical structures. With the launch of TRMM in 1997 (Kummerow et al. 2000) and CloudSat and Cloud-Aerosol Lidar and Infrared Pathfinder Satellite Observation (CALIPSO) in April 2006 (e.g., Stephens et al. 2002), we are now entering a truly active age of spaceborne remote sensing of clouds and precipitation. With this era comes a twofold challenge, one is to learn and prepare how best to use the new information from these active systems, and the second is to learn how best to optimally incorporate active and passive observations together as part of a more integrative observing system approach.

It will become obvious in the following that information about clouds and precipitation derived from seemingly different methods are in fact closely related to each other. Generally, the various products derived

from these methods are arrived at separately using the observations from sensors flown on different spacecraft, or from different sensors on the same spacecraft, or even from the measurements of different channels of the same instrument. Most often, these products are inconsistent with one another, and this lack of consistency is a source of confusion. With the combination of sensors flown on the National Aeronautics and Space Administration's (NASA) Earth Observing System (EOS) platforms, the evolution of the A-Train and the eventual emergence of the National Polar-Orbiting Operational Environmental Satellite System (NPOESS), the need for methods that optimally integrate or "assimilate" disparate observation types will only increase in the future. As we illustrate below, the development of any such assimilation methodology, however, requires a more stringent and realistic error characterization than is typically available today.

4. Examples of emission-based methods

Emission of infrared (IR) and microwave (MW) radiation to space from optically thick clouds tends to be limited to the upper portions of cloud layers. Apart from cloud-top temperature estimation, the information content contained in such emission measurements is limited. Consequently, the most useful applications of emission measurements apply to cases of optically thin cloud or precipitation layers from which the measured emission is more integrated throughout the layer in question.

Most emission methods employ the use of measurements in various atmospheric window regions of the earth's atmospheric absorption spectrum. However, a few methods seek to use measurements of emission in absorbing regions originally designed for temperature sounding. The CO_2 slicing method, for example, has been applied to IR emission measurements to map out thin cirrus clouds (e.g., Wylie et al. 2005). Recently Bauer et al. (2005) propose the use of selected MW sounding channels in addition to MW window channels for retrieving profiles of precipitation over both water and land.

Emission methods applied to optically thin media are commonly formulated using very simplistic expressions of radiative transfer often posed in terms of the transfer through a single layer in the form

$$I_{\text{obs}} = I_{\text{below}} e^{-\tau/\mu} + B(T_{\text{cld}})(1 - e^{-\tau/\mu}), \qquad (2)$$

where τ is the optical depth determined by absorption, I_{below} is the radiance of the surface and/or atmosphere below the cloud layer, and μ is cosine of the view angle. Here $B(T_{\text{cld}})$ is the Planck blackbody function defined by a "cloud" temperature T_{cld}. All emission methods revert to determining the optical depth τ from which other information about the cloud and precipitation is inferred. It will become apparent from the examples below that the largest source of uncertainty in these methods arise more from model parameters, like I_{below} and $B(T_{\text{cld}})$ in (2), than from radiance measurement uncertainties.

a. Cirrus cloud optical properties from split-window measurements

The differential absorption and emission of infrared radiation by ice crystals smaller than about 30 μm in size at two different wavelengths in the atmospheric IR window spectral region was proposed by Prabhakara et al. (1988) as a means for determining cirrus cloud optical thickness and particle size. Since then, the method has been applied extensively to satellite IR radiance data collected at or near wavelengths of 10.8 and 12 μm. The conceptual idea of the method, referred to as the split-window (SW) method, is illustrated in Fig. 3. Shown is a radiance diagram relating the quantity $\Delta T_B = T_{B,10.8} - T_{B,12}$ to $T_{B,10.8}$ where T_B is the brightness temperature of the radiance of a specified channel. The brightness temperature difference ΔT_B is related to the optical depth differences between the chosen wavelengths, which in turn is proportional to particle size; $T_{B,10.8}$ is also loosely related to optical depth and the theoretical relation between ΔT_B and $T_{B,10.8}$ form an idealized arch. Each foot of the arch is determined by the radiances I_{below} and $B(T_{\text{cld}})$ expressed in brightness temperatures and the height of the arch is related to particle size. Simplistic "inversion" methods that use this approach superimpose the observations, that is, ΔT_B and $T_{B,10.8}$, on precomputed arches and interpolation provides the basis for estimating cloud optical depth and particle size.

Although notionally simple, there are many complexities in the steps described that confound the specification of uncertainties of the approach. These include the following:

(i) The radiative transfer approximations, including the lack of infrared scattering (e.g., Stephens 1980) and the simplicity of the atmospheric model (single layer) implicit to Eq. (2) and upon which this transport equation is defined.
(ii) The specification of the forward-model parameters. For this problem, these include the lower boundary radiance I_{below} and the "cloud" temperature T_{cld}, and yet more hidden sets of parameters that relate the optical depths to particle size including effects of particle shape on these optical properties (e.g., Fig. 3b).

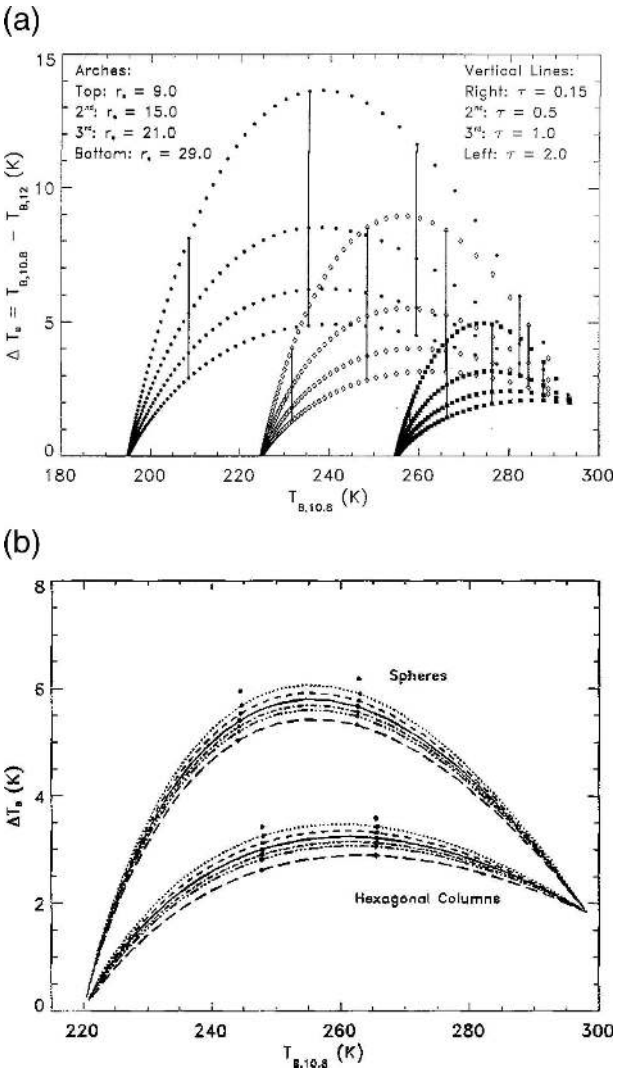

FIG. 3. (a) Theoretical brightness temperature relationships between 10.8 and 12.6 μm as a function of the corresponding brightness temperature at 10.8 μm for clouds emitting at 195, 225, and 255 K. The optical depths and effective radius are shown based on assumptions of spherical ice particles. (b) The same relationship derived for spherical and columnar ice particles. The different curves of each correspond to different assumed particle size distributions. The set of closed points correspond to an optical depth of (left) 0.5 and (right) 1.0, after Cooper et al. (2003).

Cooper et al. (2003) formulate the SW method in terms of optimal estimation inversion and use the characteristics of optimal estimation to provide an assessment of the effects of various model parameters on cirrus optical property retrievals. They show, as did Miller et al. (2000), that errors are dominated by a general lack of knowledge on the vertical location of clouds that affects the estimates of I_{below} and $B(T_{\text{cld}})$ in Eq. (2). Without specific information about where the cirrus is located in the atmospheric profile, the uncertainties on optical depth and particle size typically approach 60%–80%. With more refined information about cloud boundaries available, for example, from coincident radar and/or lidar observations and thus more accurate information on T_{cld}, the uncertainties reduce to about 10%–20%.

b. Cloud liquid water path

The differential emission of microwave radiation by clouds and water vapor at selected microwave frequencies provides the basis for estimating the vertically integrated cloud water content (LWP). This approach has mainly been applied over the global oceans (e.g., Greenwald et al. 1993; Alishouse et al. 1990; Curry et al. 1990) although methods have been developed to use these microwave emission measurements in conjunction with infrared emission measurements over land (e.g., Yeh and Liou 1983; Jones and Vonder Haar 1990; Greenwald et al. 1997).

The simple LWP retrieval approach revolves around inversion of a form of Eq. (2) with radiances, I, replaced by microwave brightness temperature,

$$\tau = -\mu \ln\left(\frac{T_{\text{obs}} - T_{\text{cld}}}{T_{\text{below}} - T_{\text{cld}}}\right), \tag{3}$$

where in this case the microwave optical depth τ is

$$\tau \approx k_v W + k_\ell \text{LWP} + \tau_{ox}. \tag{4}$$

The first term of Eq. (4) represents the water vapor contribution, which is approximately proportional to column water vapor W. The second term is the cloud liquid water droplet contributions, and the third term is due to the absorption by other gases, chiefly oxygen. Ignoring any contributions by precipitation and given microwave frequencies low enough (or conversely wavelengths large enough), then the absorbing cloud droplets behave as Rayleigh particles in which case the cloud optical depth is proportional to cloud liquid water path LWP (Stephens 1994).

Over ocean, the LWP retrieval approach uses measurements at two frequencies, one near the 22-GHz water vapor absorption line, for example at 19 GHz, and a second off the line typically at frequencies near 35 GHz. Measurements at these two frequencies, in principle, when substituted in Eq. (3) and combined with Eq. (4), then offers a way of deriving both W and LWP simultaneously, assuming all other factors are known. The inversion of Eq. (2) in the form of Eq. (3) requires a cold background surface, as over oceans, such that the differential emission between the surface and cloud is large enough to be detected above characteristic instrument noise levels. Over land, the emission from land surfaces is much larger and more variable than that

from oceans rendering the inversion of Eq. (2) in the form of Eq. (3) prone to error. Jones and Vonder Haar (1990) employ the emission at 85 GHz since clouds are optically thicker at these frequencies and the measurements are more sensitive to cloud water than are the lower frequencies. The land surface emission is characterized using the surrounding clear-sky emission and infrared estimates of skin temperature. Greenwald et al. (1997) extended the method using the polarization differences of the 85-GHz channels of the Special Sensor Microwave Imager (SSM/I) and demonstrate a greater sensitivity to the LWP of low clouds.

There are a number of complicating factors that dominate the uncertainties in the estimation of LWP by these approaches, including the following:

(i) The problem of cloud identification. This is an important part of any cloud retrieval scheme, as any misclassification of clear and cloudy scenes introduces large biases (as shown later). Unambiguous cloud detection from microwave measurements alone is most difficult given the typical large footprint of microwave radiometers.

(ii) Discriminating precipitating from nonprecipitating clouds. The assumption of Rayleigh absorption implies no precipitation-size particles present in that portion of the atmosphere observed. Simple, empirical LWP thresholds employed in both LWP retrievals and precipitation retrievals are most commonly used to classify those MW radiance scenes that are most likely to contain precipitation. In reality, drizzle and light precipitation are ubiquitous features of warm layered clouds and shallow convection (e.g., Stevens et al. 2003) and the separation between precipitation and cloud and its relationship to LWP is certainly not simple nor entirely understood. (As discussed in relation to Fig. 14, this same issue also causes parallel difficulties to the estimation of precipitation, especially in regions where aerosol influences are likely.)

(iii) Model parameters, including absorption coefficients k_v, k_ℓ, and τ_{ox}, all functions of atmospheric state, are typically parameterized in terms of surface temperature T_s. The uncertainties in these parameterizations are, however, quantifiable, and except for the cloud liquid water absorption coefficient these uncertainties are typically small relative to other sources. The cloud liquid absorption uncertainties tend to be much larger than the uncertainties of the other components because of its dependence on the uncertain cloud temperature.

(iv) The assumptions of the atmospheric model inherent to Eq. (2) require specification of the vertical location of the cloud layer as well as the water vapor structure above and below this layer. The assumed structure of the atmosphere implicit not only to this problem but also to most applications of forward models is often unrealistically simple and rarely considered as a source of error of the retrieval process.

(v) Modeling the below-cloud emission, T_{below}, mostly from the ocean or land surface, is also a complex problem. The ocean-leaving radiance is a function of ocean surface state, which in turn is dependent on ocean surface winds and other complicating factors that introduce further model parameters. The land-leaving radiances have to be accurately characterized if microwave measurements are to be used for extracting LWP information over land as the cloud signal is small relative to the background surface emissions. Effects such as soil moisture changed by recent precipitation events, for example, can introduce significant sources of error (e.g., Greenwald et al. 1997).

Although microwave radiance has been applied to estimate LWP for over 20 yr, detailed assessment of the uncertainties attached to the estimates of LWP are generally lacking. Greenwald et al. (1993) describe a sensitivity analysis for ocean-based LWP retrievals and show how the LWP retrieval errors and the factors that contribute to the errors vary according to the surface and atmospheric conditions. Their analysis considered contributions to errors from brightness temperature measurement error and model parameter error that included contributions from surface winds, sea surface temperatures, cloud temperatures, liquid water absorption coefficients (also a function of cloud temperature as noted), and the parameterization of the uniform gas contribution in Eq. (4). They estimated typical ranges of uncertainties on these parameters ignoring any possible contribution by misclassification of precipitation. With these assumptions, the LWP errors ranged from 51% for the thinnest clouds to 24% for thick clouds, the former being dominated by surface parameter uncertainties (such as surface wind errors) and the latter by cloud temperature uncertainties. Like the error estimates of other products discussed below, these errors most probably represent a lower error limit. Detailed error analysis of overland LWP retrievals has not yet been performed but some work (e.g., Diak 1995) suggest these retrievals can be subject to large errors.

The potential contaminating effects of precipitation on cloud LWP, generally ignored in most LWP studies, are illustrated in Fig. 4. An optimal estimation method developed to estimate LWP using MW radiance data

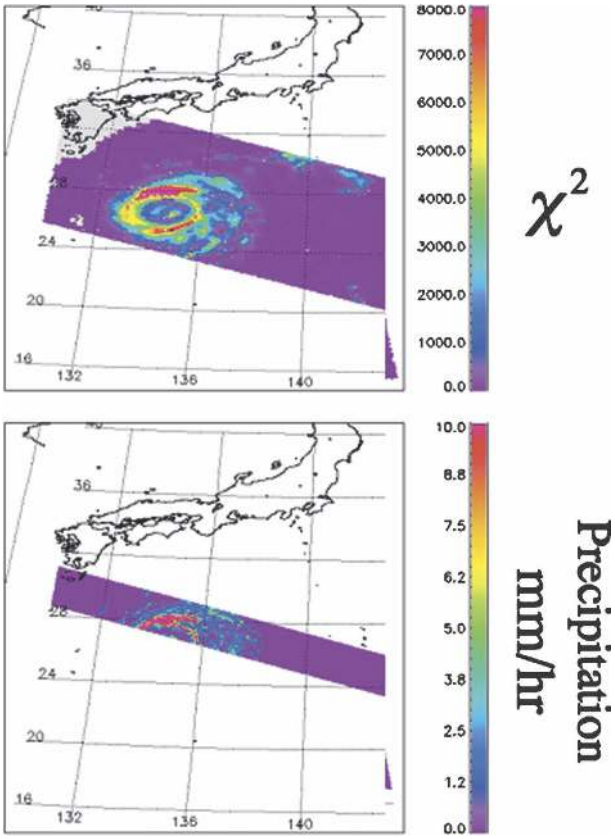

FIG. 4. The swath distribution of χ^2 (a direct measure of how well the forward model fits the observations) derived from an optimal estimation cloud LWP method developed for the TRMM TMI. Also shown is the precipitation from the equivalent swath of the TRMM PR. The largest values of χ^2 correspond to a failure of the model to fit the observations and coincide with regions of precipitation (G. S. Elsasser and C. D. Kummerow 2006, personal communication).

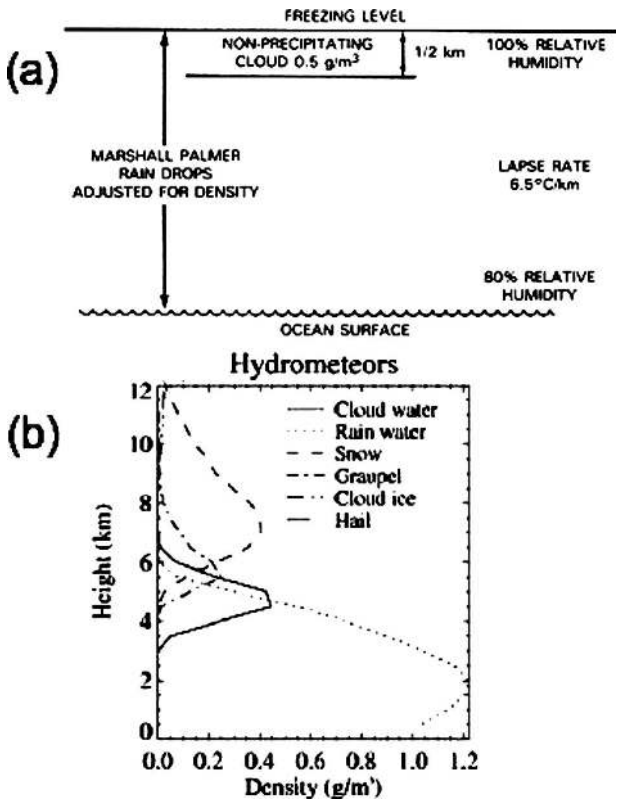

FIG. 5. (a) A simple model of the precipitating atmosphere used in the construction of the forward model as used by Wilheit (1986) for retrieving surface precipitation. (b) An example of hydrometeor profiles extracted from a cloud model as used in the GPROF method.

also provides χ^2 statistics, which is a measure of how well the "model" fits the observations. Given that most of the issues in cloud and precipitation retrieval problems revolve around the models assumed and the geophysical noise they introduce, then such information is most relevant to these retrieval problems. This information offers additional insight on the formulation of the retrieval problem as illustrated in the example of Fig. 4. For this case, the MW model of emission from low-level cloud layers poorly fits the observations when $\chi^2 > 12$ and it appears that this fit gets progressively worse (and χ^2 progressively larger) as the intensity of precipitation increases. This is illustrated in Fig. 4 where the correspondence of large values of χ^2 is shown to match regions of increasing rain rate as deduced from matching TRMM precipitation radar observations. This simple example hints at the potential value of the χ^2 retrieval diagnostic as a flag of precipitation, specifically, and more generally its value as in indicator of failure of the forward model in representing the atmosphere observed.

c. *Precipitation from microwave emission*

A number of different microwave emission algorithms have been developed over the years, each invoking slightly different forms of atmospheric model, and different solution forms of radiative transfer equation (see, e.g., Wilheit 1986 and Wilheit et al. 1994 for a general review). Figure 5 contrasts two extreme examples of the characteristics of atmospheric models constructed in forward-model simulations of radiances from precipitating cloud systems and also reflects the different nature of the retrieval state vector. The example of Fig. 5a is a very simple model of the precipitating atmosphere as used in the retrieval procedures of Wilheit et al. (1994). Despite the apparent simplicity of the model, it includes many extraneous parameters, such as the assumed lapse rate, height of the freezing level, the assumed humidity in the precipitating layer and the relationship between the ice layer properties

and the precipitation. The second example shown (Fig. 5b) is an example of the output of an entirely different model approach as used in the TRMM GPROF algorithm (e.g., Kummerow et al. 2001) that provides precipitation profiles as well as surface rain rates. Shown is one set of profiles of cloud condensate and precipitation structures derived from a cloud resolving model (CRM; Tao and Simpson 1993). These profiles are extracted from a larger library of profiles that serve as a priori inputs to the retrieval scheme. In this case, the forward model of this system is complex with uncertainties now defined not only by the radiative transfer component of the model but also by (generally unknown) errors of the CRM model and the representativeness (or lack thereof) of these CRM profiles. Bauer et al. (2005) describe a different profile retrieval scheme using combinations of microwave window and sounding channel radiances and a priori profiles of clouds and precipitation drawn from the (background) state of a forecast model of the scenes observed (see Fig. 12 and related discussion).

Many other factors contribute to the overall uncertainty of the precipitation estimates derived from microwave emission methods:

(i) Distinguishing precipitating cloudy scenes from nonprecipitating scenes. Like the cloud/no-cloud identification problem, discrimination of cloud from cloudy scenes containing precipitation is an important first step in any precipitation retrieval method and misclassification of such scenes is a source of retrieval bias. An example of how such a misclassification affects comparisons among different algorithms from the same sensors is illustrated in Fig. 6. This figure shows results from the Precipitation Intercomparison Project (PIP-2; e.g., Smith et al. 1998) applied to a swath of microwave radiance data. The different microwave emission algorithms contributing to this figure use a threshold cloud LWP to discriminate precipitation from cloud with this threshold varying from algorithm to algorithm. Shown are the percentages of all algorithms that flag a given pixel as precipitation, and for only some of the pixels do these algorithms completely agree on the occurrence of precipitation.

(ii) The nature of the atmospheric model. As noted in reference to Fig. 5, these models vary considerable in complexity and in the number and types of parameters that define them. A general sense for the influence of the atmospheric state on precipitation retrievals is provided in Fig. 7 showing simulated brightness temperatures at 10.7 GHz presented as a function of surface rain rates. The general relation between the two is primarily determined by radiative transfer, but the broad spread in this relationship is a function of the atmospheric and surface model states. The simulations shown use cloud and precipitation profiles drawn from the aforementioned GPROF database. The profiles shown in the panel to the right of Fig. 7 are those GPROF water precipitation profiles that, when input into a radiative transfer model, produce the same simulated top-of-atmosphere (TOA) microwave brightness temperature at 10.7 GHz. Clearly, no unique relation exists between the (pseudo-) measurement and the state of precipitation and cloud, which merely underscores the underconstrained nature of this retrieval problem (L'Ecuyer and Stephens 2002; Bauer et al. 2005). This ambiguity translates into significant uncertainty approaching 60% according to L'Ecuyer and Stephens (2002) and this error estimate is consistent with those of Bauer et al. (2005) who find that 80% of the retrievals they perform lie within 100% errors and 60% lie within 50% errors. One of the important future challenges for removing this troublesome ambiguity and presumably reducing uncertainty on estimating precipitation from satellites is to provide more definitive information about the atmospheric state.

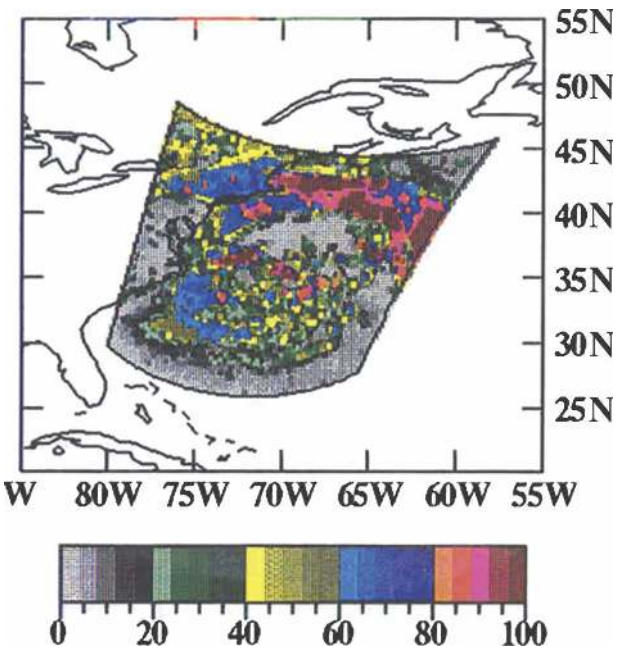

FIG. 6. The pixels of a swath of microwave radiometer data that are identified by different algorithms participating in PIP-2 as precipitation. Pixels colored 100% are those for which all algorithms agree that rain is falling at those locations.

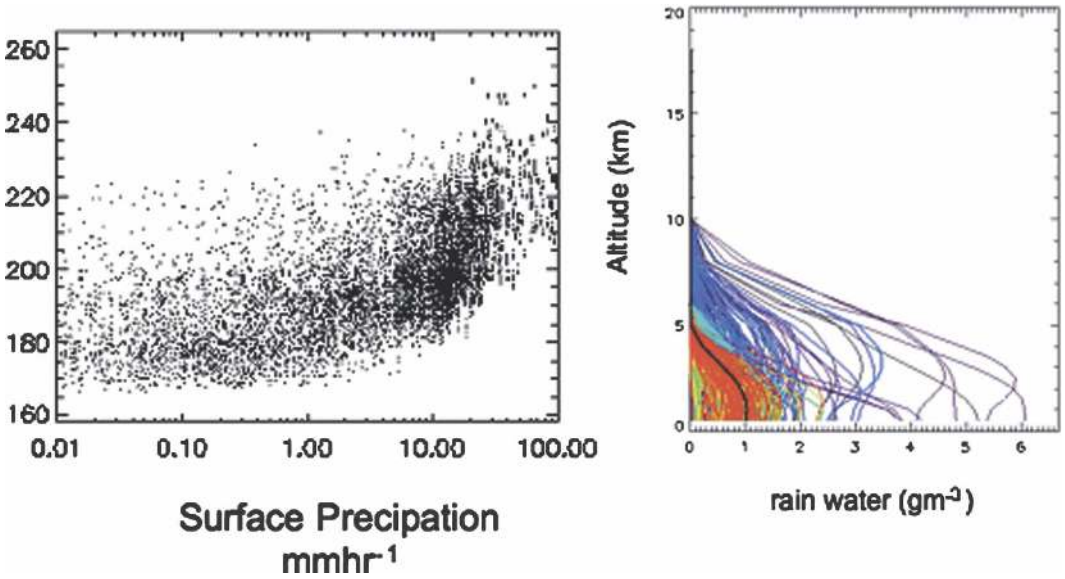

FIG. 7. (left) Illustration of the effects of atmospheric profile on TOA microwave radiances and (right) the numerous collection of profiles that give rise to a single value of the TOA brightness temperature.

(iii) Approximations to radiative transfer and rain microphysics. Uncertainties on atmospheric state form one part of the forward-model error budget. Other model error sources derive from the radiative transfer model itself, such as in the assumption of 1D geometry and in the approximations to both cloud and precipitation absorption and scattering properties. Uncertainties associated with assumptions about the microphysical properties of rainfall, including melting particles, underpin much of the geophysical noise in the system (e.g., Petty 1999; Biggerstaff et al. 2006; Fiorino and Smith 2006; Kummerow et al. 2006; among many others). A better understanding of the microphysical properties of rainfall is needed to constrain passive microwave algorithms and is one of the underlying bases of the planned Global Precipitation Mission (Smith et al. 2002). This mission concept includes a dual-frequency radar as part of the core satellite with the intent to provide a more explicit source of information about the microphysical state of the precipitation. The remote sensing not only of precipitation microphysics but also cloud microphysics and the combination of both will be an area of active research in the coming years.

5. Examples of scattering-based methods

a. Cloud optical properties from scattered sunlight

The retrieval of cloud optical properties using measurements of sunlight reflected by clouds has a relatively long history compared to some of the methods discussed previously. Sagan and Pollack (1967), for example, introduced the concept in the study of the clouds of Venus. Hansen and Pollack (1970) employ the observations of spectrally reflected sunlight made by Blau et al. (1966) to study terrestrial clouds. Twomey and Seton (1980) introduced a bispectral reflectance method (BSR) to estimate cloud optical depth and effective particle radius (r_e), and Nakajima and King (1990) popularized this method with its application to Moderate Resolution Imaging Spectroradiometer (MODIS) measurements. This approach, with some variations, has also been adopted to many other types of satellite data including *LandSat* data (Wielicki et al. 1990) and Advanced Very High Resolution Radiometer (AVHRR) radiance data (e.g., Arking and Childs 1985; Stone et al. 1990; Ou et al. 1993; Nakajima and Nakajima 1995; Platnick and Valero 1995; Han et al. 1994).

The BSR method revolves around the relation between reflection of sunlight and cloud optical depth and single-scatter albedo. Radiative transfer theory, invariably set on plane-parallel (i.e., one dimensional) geometry, predicts that the spectral reflectance from cloud layers has a general functional form:

$$\mathcal{R}_\lambda = R_\lambda(\tau, g, \varpi_o, \alpha_{sfc}, \xi, \xi_\odot), \tag{5}$$

underscoring the dependences on spectral optical depth τ; the (spectral) single-scatter albedo ϖ_o; the properties of underlying surface reflectance α_{sfc}; some characteristic of the scattering phase function as represented, for

instance, by the asymmetry parameter g; and the scattering geometry defined by the angle Θ between the incident solar radiation $\xi_\odot$ and the view direction ξ, namely $\cos\Theta = \xi_\odot \cdot \xi$. One-dimensional radiative transfer theory further predicts that the reflectance, in fact, functionally depends on the scaled optical depth, $\tau(1 - g)$ (e.g., van de Hulst 1980a,b).

The BSR approach uses narrow-band reflectances measured in two spectral regions (spectral channels). For one spectral region, characteristically at visible wavelengths, ϖ_o is assumed known since particle (and gas) absorption is negligible implying $\varpi_o = 1$. In this case the reflectance varies principally as a function of $\tau(1 - g)$. For the second channel, typically located within the near-infrared region, the solar radiation is slightly absorbed as well as scattered by cloud particles and the reflection is a function of some combination of $\tau(1 - g)$ and ϖ_o. When the two reflectance measurements are taken together, then $\tau(1 - g)$ and ϖ_o can be independently inferred under most conditions. Assuming also that g is known a priori, and surface albedo effects are adequately removed, and given some a priori relation between ϖ_o and r_e, then τ and r_e follow.

The conceptual simplicity of the BSR retrieval approach is portrayed in Fig. 8. A forward model establishes the relationships between model BSRs, τ and r_e as illustrated. The two measured reflectances then define a point superimposed on this model space that, in turn, is simply interpreted as τ and r_e through interpolation. Although simple, there are many factors that complicate the uncertainty of the method, including the following:

(i) The simplicity of the atmospheric model structure, which is typically taken to be constructed assuming one or two layers. Where the bulk of the water vapor lies relative to the cloud layer, for example, is just one of the influential assumptions of such models.

(ii) The radiative transfer model assumptions that dictate the way the BSRs are mapped to τ and r_e. The common assumption of 1D transport introduces substantial errors for retrievals applied to nonhomogeneous cloud scenes. Figure 9 from P. Gabriel (2006, personal communication) illustrates this point showing panels of data derived from a 3D large eddy simulation (LES) model (Stevens et al. 2002). Synthetic satellite radiances were produced using a 3D Monte Carlo radiative transfer model with the cloud LES data as input (left panel). The panel on the right is a mask of optical depth error obtained as the difference between the known optical depth (calculated from the LES cloud field data) and a retrieved optical depth value obtained using the synthetic radiances with a 1D radiative transfer model. The areas highlighted in white are regions of optical depth errors exceeding 50% occurring in regions where the cloud layer is broken.

(iii) Model parameter uncertainty. The BSR approach requires the identification (and removal) of all noncloud-related contributions to the measured radiances. Reflection from the surface and the added complexity of the thermal emission from the atmosphere when 3.7-μm radiances are used are two examples of these corrections. Other model parameters that influence the retrieval outcome are those parameters that define the scattering phase function, embodied, for instance, by the parameter g. The quantity $(1 - g)$ is poorly known for ice crystal clouds being influenced by the shapes, sizes, and mixtures of ice crystals that are so variable in real clouds, and a priori knowledge about them so poor, that it is generally not realistic to assert a given specific phase function such as defined from intricate scattering calculations (e.g., Yang and Liou 1998) without assigning any uncertainty attached to it. Studies such as Heidinger and

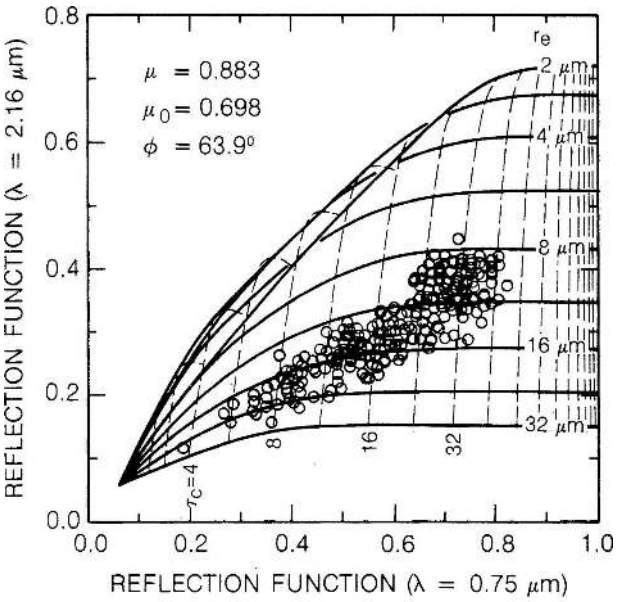

FIG. 8. Theoretical relationships between the reflection at 0.75 and 2.16 μm for various values of optical depth (vertical, dashed lines) and effective radius (solid lines) for a particular solar geometry that match aircraft data obtained during a field campaign conducted in July 1987. The theory established a gridlike relationship between reflectance, optical depth, and particle size that is nonunique at low reflectances. Data from the aircraft measurements are superimposed on this theoretical grid (from Nakajima and King 1990).

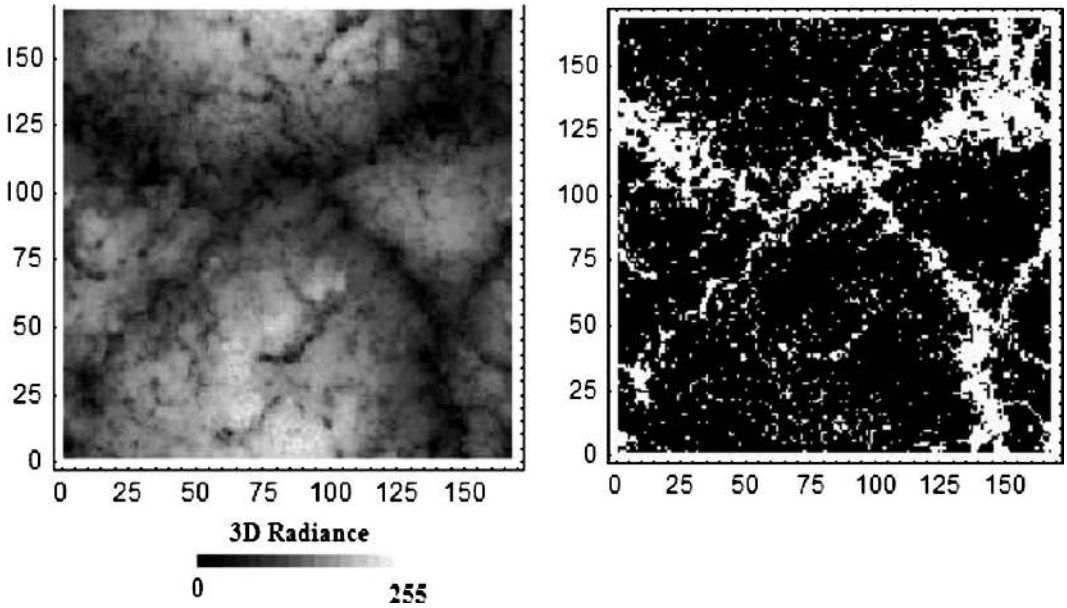

FIG. 9. A 2D plan view of visible radiances reflected by a low-level cloud layer. (left) The radiances are derived from a 3D Monte Carlo model with input from an LES model. This input defines the true optical depth. (right) A BSR retrieval of optical depth assuming 1D radiative transport produces the optical error patterns where the white pixels are errors exceeding 50%.

Stephens (2000) and Cooper et al. (2007) that attempt to account for such uncertainty suggest that these model parameter errors are dominant (50% and greater for thinner cirrus $\tau < 2$) depending on surface albedo and other atmospheric parameters but become less influential for optically thicker cirrus. Cooper et al. (2007) also show not only how the bispectral reflection relationships of Fig. 8 change dramatically through the effects of ice crystal habit on the phase function but also how this influence introduces ambiguity to the interpretation of these reflectances, further complicating the inversion process (Fig. 10). This result merely serves to highlight the grossly underconstrained nature of the ice crystal cloud optical property retrieval problem.

Platnick et al. (2004) also analyze the errors of the BSR method applied to a MODIS scene of boundary layer marine stratocumulus clouds off the Peru–Chile coast. Their study includes error contributions from measurements (assumed to be 3% for all MODIS channels) and contributions from a limited, but incomplete selection of model parameters including the specification of the surface albedo (assumed to be uncertain to 20% for all ecosystems and spectral bands) and atmospheric correction uncertainties. The principle source considered for the latter are those due to the uncertainties in specification of the above-cloud water vapor amount assumed to be uncertain to about 20%. The error estimates derived from their analysis do not include all error sources and thus represent some form of minimum system error. Their analysis indicates that the optical depth error characteristic of all low-cloud pixels is about 10% over most of the range of τ, with much larger errors occurring for smaller τ's for clouds over land because of the creeping influence of the surface

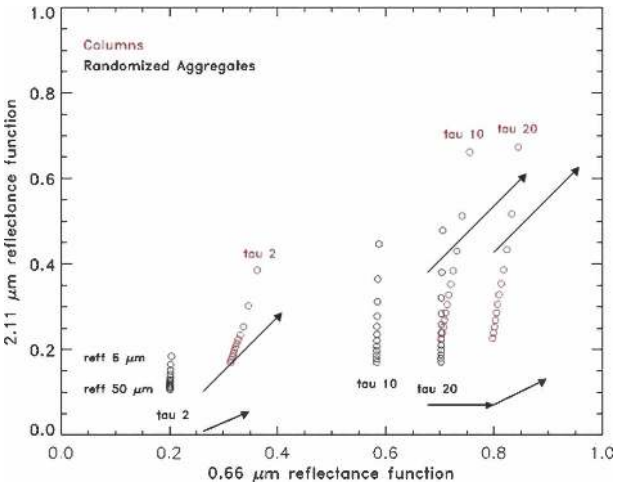

FIG. 10. The bispectral reflectance plot shown for cirrus cloud layers of different particle sizes and optical depths. The relationships are shown for two different assumed crystal habit types (adapted from Cooper et al. 2007).

albedo uncertainties. The errors on effective radius (not shown) are generally larger, approaching 20% but exceeding 100% under some conditions.

b. Microwave scattering and rainfall

As MW frequencies increase beyond about 50 GHz, the effects of scattering due to the ice particles commonly found aloft in raining clouds begins to become appreciable. At even higher frequencies, approaching the submillimeter range of wavelengths, the scattering by even smaller crystals typical of high cirrus clouds is detectable (e.g., Evans and Stephens 1995; Evans et al. 2005). The theoretical relation between microwave scattering and the ice water path (IWP) of clouds is presented in Fig. 11 for five different frequencies and for a fixed assumption about the ice crystal size distribution (from Liu and Curry 1996). As the frequency increases the sensitivity to IWP also increases. The scattering signal shown is referred to as the microwave depression—that is, the reduction in microwave radiation detected by a hypothetical satellite sensor due to the presence of a given amount of ice relative to an ice-free observation. These depressions occur from the effects of scattering that reflects upwelling microwave radiation back to the surface, thus lowering the brightness temperatures observed from space. These depressions are a strong function of assumed microphysics and typically for the types of frequencies shown in Fig. 11, the signatures observed are more related to precipitation-sized ice and depressions. Depressions of as much as 150 K can be observed over convective updrafts at 89 GHz. The sensitivity of scattering parameters to ice microphysics for precipitating systems is illustrated in Bennartz and Petty (2001).

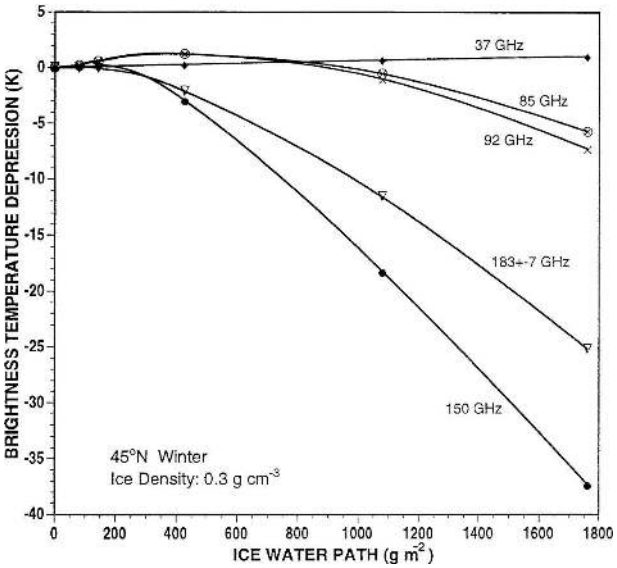

FIG. 11. Microwave brightness temperature depressions caused by scattering from layers of ice particles for selected microwave frequencies for a specific assumed size distribution of ice particles (after Liu and Curry 1996).

Empirical relationships between precipitation and these microwave brightness temperature depressions, expressed in some methods as combinations of depressions (which are referred to as "scattering indices"), are used to map out precipitation over land (Spencer et al. 1989; Kidd and Barrett 1990; Adler et al. 1994; Ferraro and Marks 1995; Conner and Petty 1998). Such relationships, however, are indirect and nonunique as highlighted in the study of Dinku and Anagnostou (2005) and vary significantly from region to region.

Unlike physically based schemes, quantifying the uncertainty of the semiempirical methods that employ simple brightness temperature indices must rely exclusively on the existence of independent validation data. This approach to error characterization has generally not proven fruitful, being complicated by many factors. Typically validation data collected from observing systems—such as surface-based networks of rain gauges, surface radar, or even airborne systems—observe precipitation on completely different spatial scales than is observed by satellites. These surface data too have their own form of uncertainties and often involve significant corrections to them (e.g., Conner and Petty 1998). Most important, however, is the lack of a unique relationship between ice scattering and rainfall, which makes validation results susceptible to variations caused by the regions in which they were performed.

Figures 12a–d are taken from the study of Bauer et al. (2005) and present a convenient contrast of the different capabilities of emission and scattering methods applied to synthetic MW measurements derived for four regions: two areas over Canada, one of frontal precipitation over the North Atlantic Ocean, and the fourth of convective precipitation over the Florida landmass. Shown is the sensitivity of the measured brightness temperatures at the frequencies defined due to (i) errors in the measurements, (ii) variabilities in surface emissivity, (iii) variabilities in liquid, and (iv) frozen precipitation. The first four frequencies represent window channels commonly used in precipitation retrievals today and the 150-GHz channel being considered by Global Precipitation Measurement (GPM) for snow retrievals (refer to next section). The other frequencies refer to sounding channels considered in that study. In the case of liquid and solid precipitation, the sensitivities shown represent a form of information content such that the larger the sensitivity with respect to the given parameter of the retrieved state (liquid and solid precipitation), the greater the information content

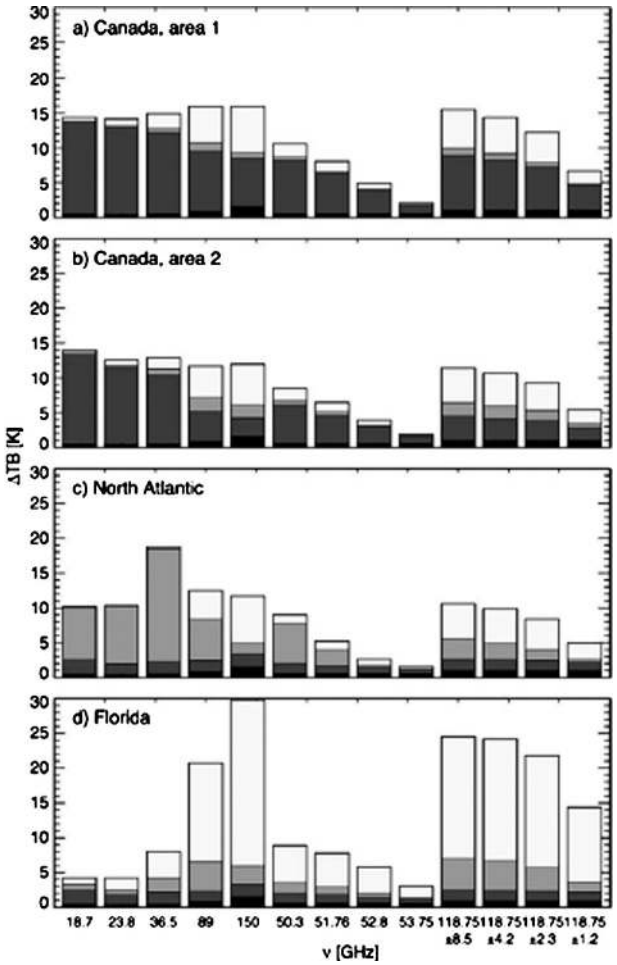

FIG. 12. The variability of the observed brightness temperature to measurement error (black), surface emissivity uncertainty (dark gray), and liquid (light gray) and frozen (white) precipitation for (a), (b) Canadian snowstorm, (c) a North Atlantic front, and (d) Florida convection (after Bauer et al. 2005).

in the measurement (e.g., L'Ecuyer et al. 2006). It is clear that for all cases in this figure the typical uncertainties of the measurements exert only a minor influence on the retrieval uncertainties. The different levels of information content of measurements over land and ocean is also clearly revealed. The sensitivity to rainfall in the two cases over Canada are very low, in part because of the low rainfall rates but also because of the lack of sensitivity of measurements over land, which is also evident in the case of convective precipitation over Florida. Only over oceans (case 3, Fig. 12c) do the lower window channels provide large sensitivity to (liquid) rainfall. The scattering channels, 89 and 150 GHz, possess disconcertingly little sensitivity to rain, a result also consistent with the marginal performances of scattering algorithms, although these channels contain greater information about lofted solid precipitation (Fig. 12d).

c. *Snowfall from microwave scattering*

Obviously the scattering signatures noted in reference to Fig. 11 also imply that it may be possible to retrieve snowfall from passive microwave scattering signatures. Because snow water contents are typically less than 1 kg m^2, Fig. 11 also makes a clear case for the need for higher-frequency microwave channels (i.e., >89 GHz) than is generally found on imaging radiometers. Indeed, most snow algorithms rely on the higher frequencies (i.e., 150, 183 GHz) used in sounding radiometers such as Advanced Microwave Sounding Unit-B (AMSU-B), Special Sensor Microwave Imager/Sounder (SSM/IS), and also planned for the GPM mission. A number of techniques exploiting the AMSU channels (e.g., Kongoli et al. 2003; Skofronick-Jackson et al. 2004) have been proposed. In addition, Bennartz and Petty (2001) have performed a detailed sensitivity analysis of scattering by various ice particles at 85 GHz on SSM/I as a precursor to a possible snow algorithm exploiting this sensor.

Similar to the precipitation retrievals using scattering methods, retrievals of snow from passive microwave sensors are fraught with uncertainties that must be made in the forward model:

(i) What are the size distributions, shapes and densities of ice particles, and how are these related to the vertical cloud development? Scattering signatures and thus the depression of T_B due to ice particles is shown clearly to be very sensitive to these assumptions (Bennartz and Petty 2001). Making progress in these areas is also the primary recommendation from an International Precipitation Working Group (IPWG) workshop (Bennartz and Ferraro 2005) defining needs for improved snowfall retrievals in the future.

(ii) What is the nature of the below-cloud emission? Snow has often accumulated on the ground and this poses serious problems when trying to identify the below-cloud emission. In addition, the snow on the ground has similar scattering properties as the snow aloft (snow identification problem), but its emissivity is a strong function of its temporal evolution and thus difficult to model (Kelly et al. 2004). While water vapor channels such as the 183-GHz spectral channels on AMSU-B become opaque to the surface when enough water vapor is present, even the center frequency is sensitive to the ground under very dry conditions.

(iii) The assumptions about the atmospheric model be-

come important when the water vapor (i.e., 183 GHz) channels are used. In particular, the water vapor above the snow cloud must be known if the scattering signatures are to be physically interpreted.

6. Multisensor product comparison and methods

The examples of the previous sections show how apparently the same parameters are derived from different measurement types and retrieval schemes based on different physics. This raises a number of questions:

(i) To what extent can comparisons of retrievals of the same parameters, based on entirely different physical assumptions, identify problem areas of individual methods?
(ii) To what extent can comparisons be used quantitatively to evaluate these retrieval assumptions?
(iii) To what extent do differences or inconsistencies reflect different information contained in the combination of observations? Stated differently, is there more information to be obtained from the combination of different measurement types than is available from the sum of individually applied retrievals?
(iv) If different observations are to be combined on the basis of information content, what then do we mean by information, how do we define its content quantitatively and how should this information guide the blending of observations (e.g., L'Ecuyer et al. 2006)?

The combination and blending of different types of observations serve as the basis of the ISCCP and GPCP programs so the value of combining observations has long been realized. ISCCP, for example, combines measurements of IR emission and scattered sunlight to characterize clouds and GPCP blends MW and IR emission measurements of precipitation. Here we provide further examples of comparisons of cloud and precipitation products derived from different but matched observations in an attempt to begin to address some aspects of these questions.

a. The LWP example

The optical depth–effective radius information derived from the BSR method can be combined to deduce the cloud LWP through the relation (Stephens 1978)

$$\tau \approx \frac{3}{2}\frac{\mathrm{LWP}}{r_e}.$$

Simultaneous measurements of the spectral reflectances and MW radiances, such as available from MODIS and the Advanced Microwave Scanning Radiometer (AMSR) for EOS (AMSR-E) instrument on *Aqua*, provides an opportunity to compare the two different inferences on LWP based on entirely different physical assumptions. Comparisons of low-cloud LWP retrieved by these two different approaches applied to data obtained simultaneously from MODIS and AMSR-E are reproduced in Fig. 13 (from T. J. Greenwald et al. 2006, personal communication). The comparisons are shown as probability distribution functions of the differences between LWP obtained from AMSR-E radiances and from MODIS reflectances matched to the AMSR-E 37-GHz channel footprint. The LWP comparisons apply to nonprecipitating scenes deemed so by AMSR-E observations. The comparisons reveal a systematic and repeatable bias between the LWP obtained by both methods. The bias, of order 50 gm^{-2}, is substantial when measured in terms of solar energy reflected by such clouds.

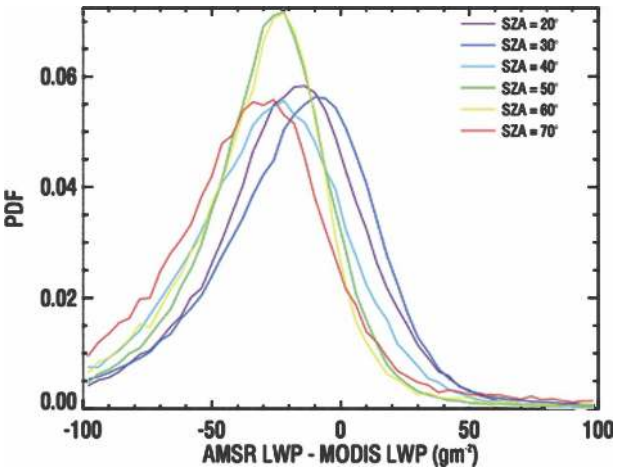

FIG. 13. Comparison AMSR-E cloud LWP and the MODIS-derived LWP for matched footprints and for nonprecipitating clouds and grouped by different solar zenith view angles (SZA; T. J. Greenwald et al. 2006, personal communication).

Figure 14 provides another perspective on the biases revealed in Fig. 13 but in this case the data shown apply to TRMM and TRMM Microwave Imager (TMI) observations. Shown is the LWP distribution taken from the version-3a TMI Ocean Products when all Visible and Infrared Scanner (VIRS) pixels within the TMI footprint are deemed to be cloud free. The significant amounts of cloud water retrieved from the TMI measurements under cloud free conditions point to problems with cloud misidentification in the TMI.

b. TRMM TMI and PR comparisons

Precipitation products derived from TRMM observations include precipitation derived independently from

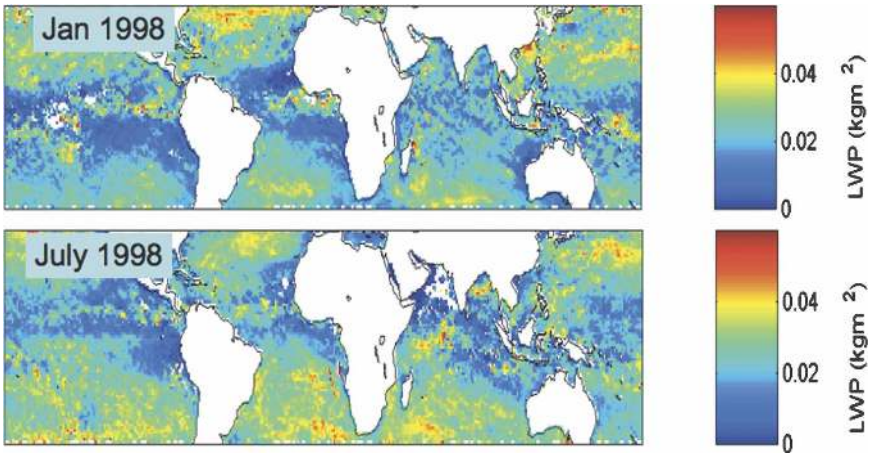

FIG. 14. The TMI-deduced distribution of cloud LWP for those scenes determined by all VIRS pixels within the TMI footprint to be clear (T. J. Greenwald et al. 2006, personal communication).

both the precipitation radar (PR) and TMI as well as precipitation derived from the combination of these observations. The two instrument-centric products are expected to contain significant random variations because of the differences in view angle, spatial resolution, and information content of the different sensors, but when averaged over time and space many of these differences should disappear. However, comparisons between the two rainfall products averaged on time and space scales pertinent to climate studies reveal systematic differences between the two that do not disappear with averaging. Berg et al. (2006), for instance, find regional and seasonal signatures of differences that are correlated to the total precipitable water for reasons not yet understood. Robertson et al. (2003) suggest that climatological discrepancies between the active and passive

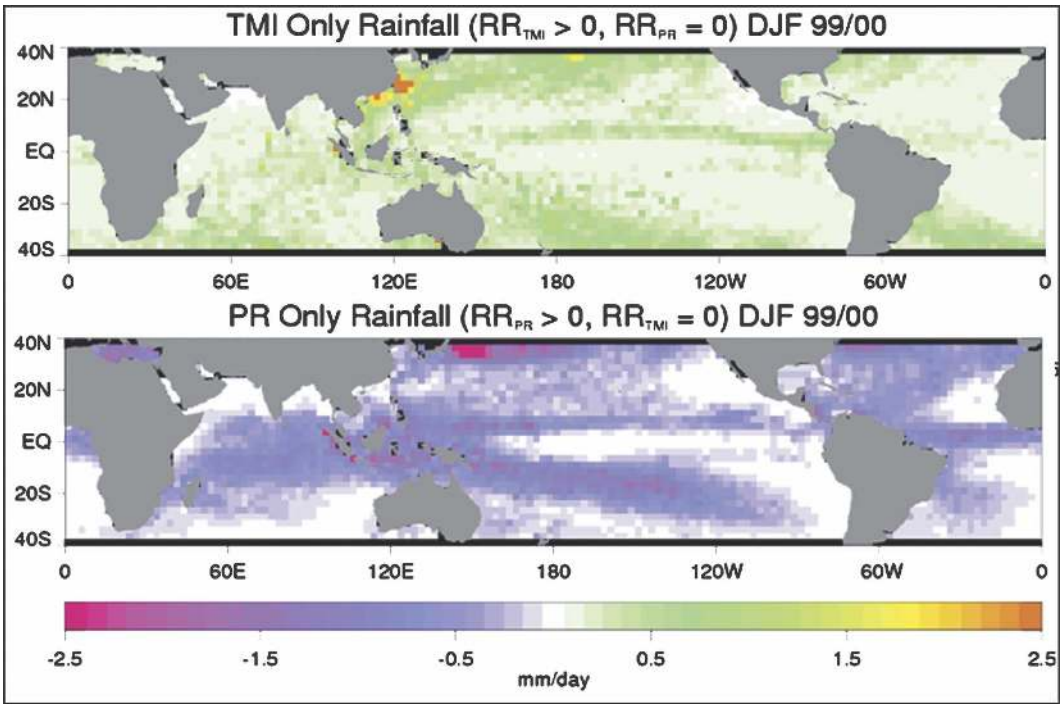

FIG. 15. Comparison of the precipitation derived from (top) TMI pixels when the PR indicates no returns and conversely the (bottom) PR precipitation when the TMI algorithm indicates no precipitation (Berg et al. 2006).

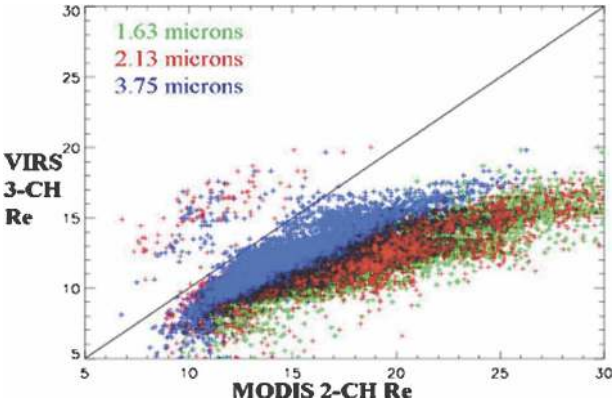

FIG. 16. Example of a comparison of the three MODIS effective radius (two channel) products (identified by the near-infrared channel used) compared to a new three-channel retrieval scheme developed for VIRS for layered water clouds over the ocean.

TRMM rainfall products during the ENSO event of 1997/98 could in part be explained by assumptions made in precipitation microphysics in retrievals.

Figure 15 is taken from the study of Berg et al. (2006) and shows precipitation derived from TRMM TMI (top) and PR (bottom) observations when the other respective sensor (PR for the results of the upper panel and TMI for the lower panel) indicates no precipitation. In this way, the differences shown highlight the problems with rainfall detectability associated with both methods. Comparisons reveal, for example, that the TMI consistently misses rainfall events behind cold fronts in the extratropics, presumably because of the fact that these systems are spatially too small to be properly captured by the relatively large TMI footprints. Regions also exist where the TMI consistently identifies rainfall when the PR detects none. Such differences can occur as a result of misclassification of precipitation within the TMI footprint and can also occur through the lack of sensitivity of the PR in light rain. The differences, notably in regions of high levels of aerosols (such as off the east coast of the Asian continent), hint at the possible influence of aerosols on precipitation in these regions. Further analysis (not shown) reveals that such regions contain extremely high liquid water contents but are not precipitating. These water contents fall well above the rain/no rain LWP threshold used to flag precipitation and are mistakenly interpreted as rain.

Another synergy that has recently been exploited is the adjustment of the median volume diameter, D_0, by the passive microwave radiometer when precipitation is light. In this case, the PR cannot exploit the surface reference technique and the median volume diameter is essentially the assumed value. This initial guess of the rainwater content can be used to simulate radiances and, if not consistent with the observed TMI radiances, can be used to adjust D_0 to make both measurements more consistent as in Masunaga and Kummerow (2005) or Grecu and Olson (2006).

c. Low cloud effective radius

Low cloud effective radius derived from three different combinations of MODIS channels is shown in Fig. 16. The results apply to a low cloud layer, and the MODIS-derived values are compared to the r_e obtained from a retrieval scheme that uses matched TRMM VIRS observations. The particle sizes retrieved vary significantly—not only between VIRS and MODIS but between the different MODIS products themselves, in some cases by as much as a factor of 2. At first glance, it is not clear as to whether these differences result from different retrieval assumptions or whether they reflect some other characteristic of the physical world not represented by the physical retrieval model.

The effective radius quantities derived from the BSR method are vertically averaged quantities with the averaging dictated by the weighting function characteristic of the specific spectral channels used (e.g., Platnick 2000; Chang and Li 2002). The characteristics of these functions suggest that the particle size derived using different channel combinations (e.g., the 0.75–2.2-μm channel combination versus the 0.75–3.7-μm combination) are weighted differently, with information coming from different levels within the clouds. Chang and Li (2003) employ a version of the BSR method with different combinations of channels and use the differences in r_e like those of Fig. 17 to provide some measure of the vertical profile of effective radius in clouds. Chen et al. (2007) further demonstrate a correlation between the sign of the difference between particle sizes at cloud top and base and the presence of precipitation (Fig. 17). The results shown on this diagram are consistent with the existence of larger precipitation drops low in the cloud that are apparently detectible from near-infrared measurements of sunlight reflected by clouds. This example demonstrates, in a small way, the value of joint observations of cloud and precipitation in studying the precipitation-related processes.

d. Cirrus cloud optical properties

The output states of both the SW and BSR methods are the optical depths and effective radii of thin cirrus clouds. Using MODIS airborne simulator (MAS) data obtained during the Cirrus Regional Study of Tropical Anvils and Cirrus Layers-Florida Area Cirrus Experiment (CRYSTAL-FACE), Cooper et al. (2007) con-

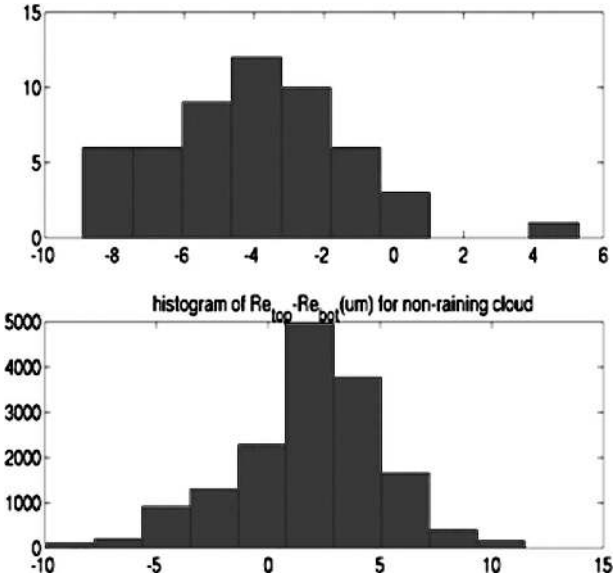

FIG. 17. The histogram of effective radius differences as a function of precipitation as detected by the PR (Z. Li 2006, personal communication).

trast the properties derived from these two methods for a cloud observed on 23 July 2004. At approximately 1830 UTC, the ER-2 over flew a progressively thickening cirrus cloud shield off the east coast of Florida as is indicated by the combined airborne lidar (CPL) and cloud radar (CRS) observations shown in Fig. 18. Figures 19a and 19b present retrieved effective radius and ice water path (in this case, a combination of optical

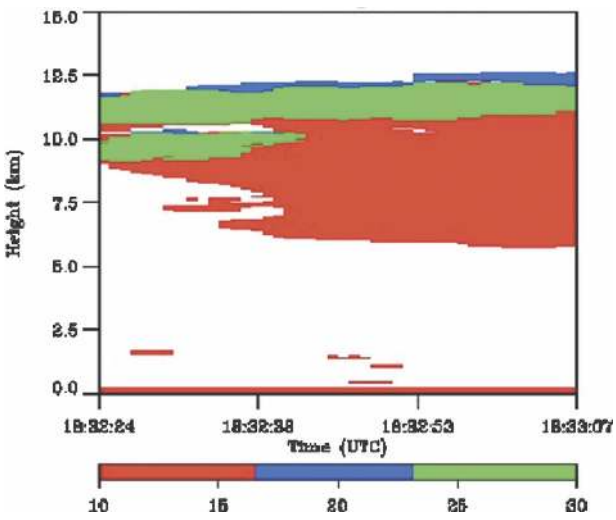

FIG. 18. Composite of airborne lidar and radar observations of clouds. The red indicates portions of clouds detected by radar only, the blue indicates where the lidar detected cirrus but the radar did not, and the green indicates that portion of the cirrus where both sensors detected cirrus.

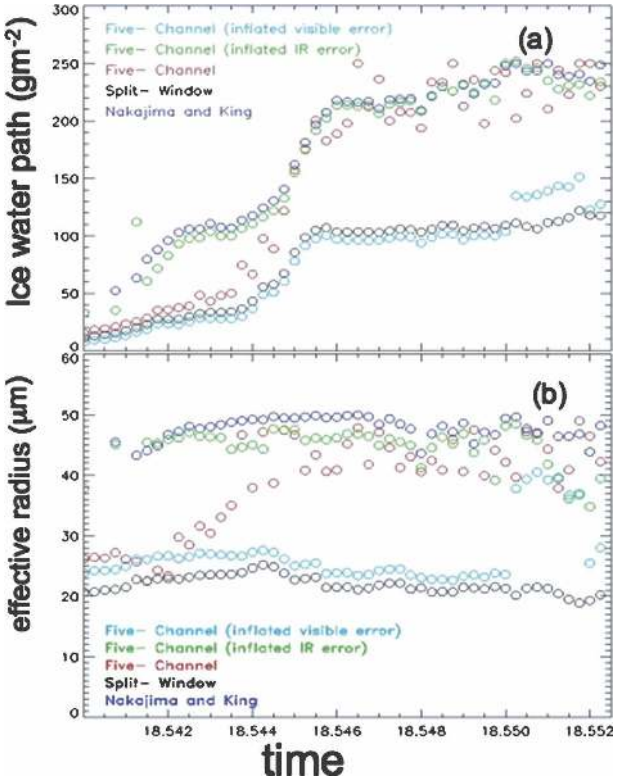

FIG. 19. The retrieval of (a) cloud ice water path and (b) effective radius derived from MODIS airborne simulator data. Five different retrieval versions are shown, modified from Cooper et al. 2007.

depth and effective radius) as a function of the alongtrack position of the aircraft matching the same period of time of Fig. 18. These retrieved quantities are derived from three different algorithms: one corresponds to results from a two-channel BSR method analogous to that of Nakajima and King (1990), a second to results from a two-channel SW method, and a third is from a method that incorporates five channels that include both the SW and BSR channels. Retrieval results show clearly how different are the estimates of effective radius between the two methods (Fig. 19b), and it is not obvious a priori which one is more realistic. The five-channel method weights the channel information differently according to how model errors are specified. The smooth transition of the solution of this five-channel method from the SW to the BSR as optical depth increases occurs as a consequence of this error specification. For thin cirrus, the phase-function errors exert such an influence on the BSR method that the solution tends to be weighted toward the SW method, since, in this case, the cloud location and hence cloud temperature is known, producing errors that are smaller than those of the BSR. As the cloud thickness in-

creases, the SW method becomes less reliable because of the lack of sensitivity of the method that enhances its related error, such that the solution now tracks the BSR method, which now is less prone to phase-function error under these thick cloud conditions.

The important message conveyed in the example of Fig. 19 is that any blending of different types of observations requires a proper disclosure of retrieval errors as these largely establish the relative weighting of the different observations used in the blending. Poorly specified errors result in improperly weighted observations. As a way of underscoring this point, the retrievals of Figs. 19a and 19b were repeated using two different error assumptions in the five-channel scheme, and both are also shown in Figs. 19a and 19b. One assumption adds substantial error to that part of the model that represents the SW channels. In this case, the solution indicated as on the figure resembles more closely the original BSR result. Conversely, the second assumption shifts error to the portion of the model associated with the BSR channels, with the result that the solution now resembles the SW solution.

e. Active and passive: A CloudSat example

The benefit of combining active and passive observations for deriving cloud and precipitation properties has been demonstrated for more than 20 yr using measurements from both aircraft- and ground-based lidar, radar, and radiometer systems (e.g., Platt et al. 1998; Matrosov et al. 1992; Mace et al. 1998; Skofronick-Jackson et al. 2003; and many others). The value of this sort of combination of observations is also emerging from TRMM, with the kinds of studies described above.

The complementary nature of the active and passive measurements is exploited in the CloudSat liquid water and ice water content algorithms that combine radar observations with MODIS radiance data. The essence of the method is illustrated in Fig. 20a, which presents graphically the relation between integrated radar reflectivity I_Z and optical depth on cloud LWP and geometric mean particle size r_g. These relationships are as follows (see Austin and Stephens 2001 for details):

$$\ln I_Z \propto \ln\mathrm{LWP} + 3\ln r_g,$$

$$\ln\tau \propto \ln\mathrm{LWP} - \ln r_g,$$

where

$$I_Z = \int_{z_{\mathrm{base}}}^{z_{\mathrm{top}}} Z(z)\,dz.$$

Contours of constant particle size r_g and LWP are shown as functions of I_Z and τ in Fig. 20a. The near orthogonality of the contours graphically indicates that

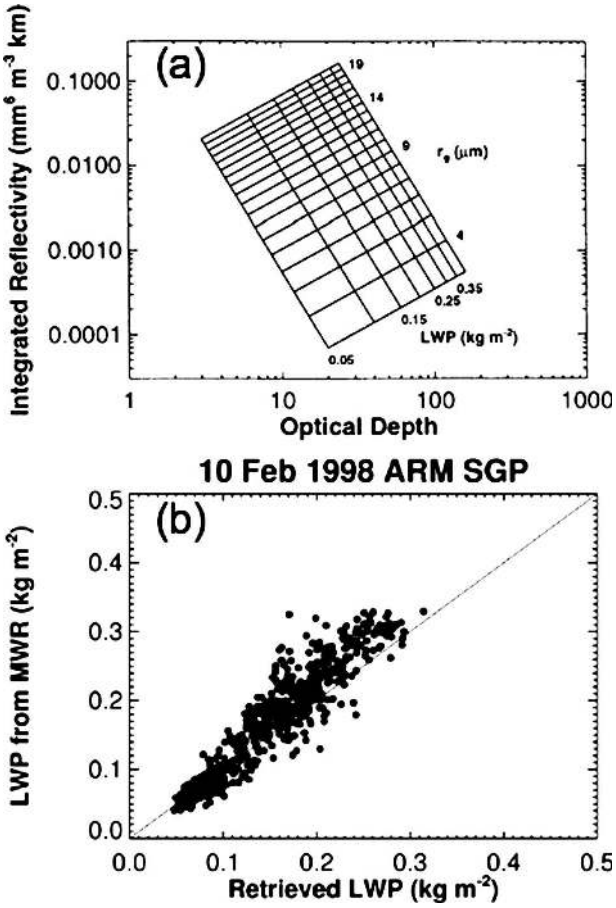

FIG. 20. (a) Relation between geometric mean radius r_g, liquid water path W, integrated reflectivity I_Z, and optical depth τ for a hypothetical 1-km stratus cloud with uniform r_g. (b) Comparison of cloud liquid water path retrieved from radar plus visible optical depth (RVOD) retrieval and value retrieved from microwave radiometer (MWR) data (Austin and Stephens 2001).

measurements of I_Z and reflection measurements in the form of τ contain independent information about r_g and LWP. Austin and Stephens (2001) develop a retrieval method that combines both pieces of information to obtain r_g and W. An example of an optimal estimation retrieval obtained using this method applied to data collected at the Atmospheric Radiation Measurement Program (ARM) southern Great Plains site is provided in Fig. 20b, in which values of LWP retrieved from a combination of cloud radar and optical depth data are compared to LWP values retrieved from a microwave radiometer.

7. Summary

This paper presents a critical review of a number of popular methods that have been developed to retrieve cloud and precipitation properties from satellite radi-

ance measurements. Properties typically derived from these measurements may be classified into two broad types: cloud optical properties that characterize the interaction of clouds with radiation, and water content properties of clouds and precipitation. One common thread that affects retrievals of both types of properties are the necessary, simplifying assumptions introduced for the microphysical properties of clouds and precipitation.

The emphasis of the paper concerns the nature of retrieval uncertainties, as these shape future data assimilation applications in the form of direct radiance assimilation, product assimilation, or even in the use of retrieved information as a source of model error characterization. It is demonstrated throughout the paper how cloud and precipitation observing systems developed around seemingly simple methods of retrievals are in fact very complex, which thus explains, in part, why assigning realistic errors to the properties derived from them has been so elusive in the past. Two primary sources of error, common to the cloud and precipitation retrieval problem, that define the overall uncertainty of the observing system were stressed:

(i) Errors associated with the identification of cloudy scenes from clear scenes and the identification of precipitation in cloudy scenes from nonprecipitating cloudy scenes. Examples of problematic discrimination of cloud clear were highlighted in the case of MW estimates of cloud liquid water path (Figs. 13 and 14), in which unphysical biases in the LWP information were shown in regions that were most probably clear. The problem of precipitation discrimination too was evident in the examples of Figs. 6 and 15, underscoring problems with overly simplistic methods of separating cloud from precipitation based primarily on simple LWP thresholds. A more unified approach to observing clouds and precipitation properties jointly would clearly help such problems.

(ii) Errors introduced by the forward model and its related parameters. The forward model generally contains two main components: a model of the atmosphere and the cloud and precipitation structures imbedded in that atmosphere, and a forward model of the radiative transfer that produces the synthetic measurement that is ultimately compared to the measurement. The vast majority of methods developed for deriving cloud and precipitation information from satellite measurements are highly sensitive to these model parameters, which merely reflects the underconstrained nature of the problem and the essential nature of other information.

The cloud and precipitation retrieval examples presented in this paper tend to be constructed around very unrealistic atmospheric models typically composed of just a few layers. The consequence is that the retrievals become highly sensitive to the unobserved parameters of those layers and the atmosphere above and below. For example, the MW-emission-based LWP method and the IR SW cirrus cloud optical property method were shown to be very sensitive to the assumptions about the temperature of the cloud layer, which contribute significantly to retrieval errors. Cloud methods based on scattered sunlight also are highly sensitive to assumptions of the model, including the inherent form of radiative transfer model (e.g., Fig. 9 and discussion) as well as heavy reliance on poorly known specific model parameters (e.g., Fig. 10). Assumptions of the vertical cloud and precipitation structures (Fig. 7) as well as the details of ice particle properties and size distributions are a dominant source of uncertainty in the estimation of precipitation. Clearly a better definition of the atmospheric state, and the vertical structure of clouds and precipitation are needed to improve the information extracted from satellite observations. The combination of active and passive measurements, briefly touched on in section 6, offers much scope for improving cloud and precipitation retrievals.

We also suggest that we are embarking on a new age of remote sensing of clouds and precipitation, starting with TRMM and continuing on with the A-Train, and that this new age provides us with the opportunity to move away from present artificial practices of "observing" and analyzing clouds and precipitation as separate entities. A more unified approach to observing clouds and precipitation properties jointly, for many reasons illustrated in this paper, would not only greatly improve these retrieval problems but also advances our understanding of important cloud and precipitation processes.

Acknowledgments. Aspects of this work have been supported under various grants including NASA Grants NAS5-99237, NAG5-11475, NAG5-13640, and DOE Research Grant DE-FG02-05ER63961. We also want to acknowledge the contributions of P. Gabriel, S. Cooper, W. Berg, T. L'Ecuyer, T. Greenwald, and Z. Li.

REFERENCES

Adler, R. F., G. J. Hufmann, and P. R. Keehn, 1994: Global tropical rain estimates from microwave adjusted geosynchronous IR data. *Remote Sens. Rev.,* **11,** 125–152.

——, and Coauthors, 2003: The version-2 Global Precipitation Climatology Project (GPCP) monthly precipitation analysis (1979–present). *J. Hydrometeor.,* **4,** 1147–1167.

Alishouse, J. C., J. B. Snider, E. R. Westwater, C. T. Swift, C. S. Ruf, S. A. Vongsathron, and R. R. Ferraro, 1990: Determination of cloud liquid water content using the SSM/I. *IEEE Trans. Geosci. Remote Sens.,* **28,** 817–822.

Arking, A., and J. D. Childs, 1985: Retrieval of cloud cover parameters from multispectral images. *J. Climate Appl. Meteor.,* **24,** 322–333.

Austin, R. T., and G. L. Stephens, 2001: Retrieval of stratus cloud microphysical parameters using millimeter-wave radar and visible optical depth in preparation for CloudSat. 1. Algorithm formulation. *J. Geophys. Res.,* **106,** 28 233–28 242.

Bauer, P., E. Moreau, and S. Di Michele, 2005: Hydrometeor retrieval accuracy using microwave window and sounding channel observations. *J. Appl. Meteor.,* **44,** 1016–1032.

Benedetti, A., G. L. Stephens, and J. M. Haynes, 2003: Ice cloud microphysics retrievals from millimeter radar and visible optical depth using an estimation theory approach. *J. Geophys. Res.,* **108,** 4335, doi:10.1029/2002JD002693.

Bennartz, R., and G. W. Petty, 2001: The sensitivity of microwave remote sensing observations of precipitation to ice particle size distribution. *J. Appl. Meteor.,* **40,** 345–364.

——, and R. Ferraro, cited 2005: Report on the IPWG/GPM/GRP workshop on global microwave modeling and retrieval of snowfall. [Available online at http://www.isac.cnr.it/~ipwg/reports.html.]

Berg, W., T. L'Ecuyer, and C. Kummerow, 2006: Rainfall climate regimes: The relationship of regional TRMM rainfall biases to the environment. *J. Appl. Meteor. Climatol.,* **45,** 434–454.

Biggerstaff, M. I., E.-K. Seo, S. V. Hristova-Veleva, and K.-Y. Kim, 2006: Impact of cloud microphysics on passive microwave retrievals of cloud properties. Part I: Model comparison using EOF analyses. *J. Appl. Meteor. Climatol.,* **45,** 930–954.

Blau, H. H., R. P. Espinola, and E. C. Reifenstein III, 1966: Near infrared scattering by sunlit terrestrial clouds. *Appl. Opt.,* **5,** 555–564.

Chang, F.-L., and Z. Li, 2002: Estimating the vertical variation of cloud droplet effective radius using multispectral near-infrared satellite measurements. *J. Geophys. Res.,* **107,** 4257, doi:10.1029/2001JD000766.

——, and ——, 2003: Retrieving vertical profiles of water-cloud droplet effective radius: Algorithm modification and preliminary application. *J. Geophys. Res.,* **108,** 4763, doi:10.1029/2003JD003906.

——, and ——, 2005: A near-global climatology of single-layer and overlapped clouds and their optical properties retrieved from *Terra*/MODIS data using a new algorithm. *J. Climate,* **18,** 4752–4771.

Chen, R., F.-L. Chang, Z. Li, R. Ferraro, and F. Weng, 2007: Impact of the vertical variation of cloud droplet size on the estimation of cloud liquid water path and rain detection. *J. Atmos. Sci.,* **64,** 3843–3853.

Conner, M. D., and G. W. Petty, 1998: Validation and intercomparison of SSM/I rain-rate retrieval methods over the continental United States. *J. Appl. Meteor.,* **37,** 679–700.

Cooper, S. J., T. L'Ecuyer, and G. L. Stephens, 2003: The impact of explicit cloud boundary information on ice cloud microphysical property retrievals from infrared radiances. *J. Geophys. Res.,* **108,** 4107, doi:10.1029/2002JD002611.

——, ——, P. Gabriel, A. J. Baran, and G. L. Stephens, 2007: Performance assessment of a five-channel estimation based ice cloud retrieval scheme for use over the global oceans. *J. Geophys. Res.,* **112,** D04207, doi:10.1029/2006JD007122.

Curry, J. A., C. D. Ardeel, and L. Tian, 1990: Liquid water content and precipitation characteristics of stratiform clouds as inferred from satellite microwave measurements. *J. Geophys. Res.,* **95,** 16 659–16 671.

Diak, R. G., 1995: Column cloud liquid water amounts for nonprecipitating clouds versus an effective cloud fraction derived from microwave data: A simulation study. *J. Atmos. Oceanic Technol.,* **12,** 960–969.

Dinku, T., and E. Anagnostou, 2005: Regional differences in overland rainfall from PR-calibrated TMI algorithm. *J. Appl. Meteor.,* **44,** 189–205.

Evans, K. F., and G. L. Stephens, 1995: Microwave radiative transfer through clouds composed of realistically shaped ice crystals. Part II: Remote sensing of ice clouds. *J. Atmos. Sci.,* **52,** 2058–2072.

——, J. Turk, T. Wong, and G. L. Stephens, 1995: A Bayesian approach to microwave precipitation profile retrieval. *J. Appl. Meteor.,* **34,** 260–278.

——, S. J. Walter, A. J. Heymsfield, and G. M. McFarquhar, 2002: Submillimeter-wave cloud ice radiometer: Simulations of retrieval algorithm performance. *J. Geophys. Res.,* **107,** 4028, doi:10.1029/2001JD000709.

——, J. R. Wang, P. E. Racette, and G. Heymsfield, 2005: Ice cloud retrievals and analysis with the compact scanning submillimeter imaging radiometer and the cloud radar system during CRYSTAL-FACE. *J. Appl. Meteor.,* **44,** 839–859.

Ferraro, R. R., and G. F. Marks, 1995: The development of SSM/I rain-rate retrieval algorithms using ground-based radar measurements. *J. Atmos. Oceanic Technol.,* **12,** 755–770.

Fiorino, S. T., and E. A. Smith, 2006: Critical assessment of microphysical assumptions within TRMM radiometer rain profile algorithm using satellite, aircraft, and surface datasets from KWAJEX. *J. Appl. Meteor. Climatol.,* **45,** 754–786.

Grecu, M., and W. S. Olson, 2006: Bayesian estimation of precipitation from satellite passive microwave observations using combined radar radiometer retrievals. *J. Appl. Meteor. Climatol.,* **45,** 416–433.

Greenwald, T. J., G. L. Stephens, T. H. Vonder Haar, and D. L. Jackson, 1993: A physical retrieval of cloud liquid water over global oceans using special sensor microwave/imager (SSM/I) observations. *J. Geophys. Res.,* **98,** 18 471–18 488.

——, C. L. Combs, A. S. Jones, D. L. Randel, and T. H. Vonder Haar, 1997: Further developments in estimating cloud liquid water over land using microwave and infrared satellite measurements. *J. Appl. Meteor.,* **36,** 389–405.

Han, Q., W. B. Rossow, and A. A. Lacis, 1994: Near-global survey of effective droplet radii in liquid water clouds using ISCCP data. *J. Climate,* **7,** 465–497.

Hansen, J., and J. B. Pollack, 1970: Near-infrared light scattering by terrestrial clouds. *J. Atmos. Sci.,* **27,** 265–281.

Heidinger, A., and G. L. Stephens, 2000: Molecular line absorption in a scattering atmosphere. Part II: Application to remote sensing in the O_2 A-band. *J. Atmos. Sci.,* **57,** 1615–1634.

Jacobowitz, H., L. L. Stowe, G. Ohring, A. Heidinger, K. Knapp, and N. R. Nalli, 2003: The Advanced Very High Resolution Radiometer pathfinder atmosphere (PATMOS) climate dataset: A resource for climate research. *Bull. Amer. Meteor. Soc.,* **84,** 785–793.

Jones, A. S., and T. H. Vonder Haar, 1990: Passive microwave remote sensing of cloud liquid water over land regions. *J. Geophys. Res.,* **95,** 16 673–16 683.

Kelly, R. E. J., N. A. Drake, and S. L. Barr, Eds., 2004: *Spatial Modelling of the Terrestrial Environment*. John Wiley and Sons, 276 pp.

Kent, G. S., D. M. Winker, M. T. Osborn, M. P. McCormick, and K. M. Skeens, 1993: A model for the separation of cloud and aerosol in SAGE II occultation data. *J. Geophys. Res.,* **98,** 20 723–20 735.

Kidd, C., and E. C. Barrett, 1990: The use of passive microwave imagery in rainfall monitoring. *Remote Sens. Rev.,* **4,** 415–450.

Kongoli, C., P. Pellegrino, R. R. Ferraro, N. C. Grody, and H. Meng, 2003: A new snowfall detection algorithm over land using measurements from the Advanced Microwave Sounding Unit (AMSU). *Geophys. Res. Lett.,* **30,** 1756, doi:10.1029/2003GL017177.

Kummerow, C., and Coauthors, 2000: The status of the Tropical Rainfall Measuring Mission (TRMM) after two years in orbit. *J. Appl. Meteor.,* **39,** 1965–1982.

——, and Coauthors, 2001: The evolution of the Goddard Profiling Algorithm (GPROF) for rainfall estimation from passive microwave sensors. *J. Appl. Meteor.,* **40,** 1801–1820.

——, W. Berg, J. Thomas-Stahle, and H. Masunaga, 2006: Quantifying global uncertainties in a simple microwave rainfall algorithm. *J. Atmos. Oceanic Technol.,* **23,** 23–37.

L'Ecuyer, T. S., and G. L. Stephens, 2002: An uncertainty model for Bayesian Monte Carlo retrieval algorithms: Application to the TRMM observing system. *Quart. J. Roy. Meteor. Soc.,* **128,** 1713–1737.

——, P. Gabriel, K. Leesman, S. Cooper, and G. Stephens, 2006: Objective assessment of the information content of visible and infrared radiance measurements for cloud microphysical property retrievals over the global oceans. Part 1: Liquid clouds. *J. Appl. Meteor. Climatol.,* **45,** 20–41.

Liu, G., and J. A. Curry, 1996: Large-scale cloud features during January 1993 in the North Atlantic Ocean as determined from SSM/I and SSM/T2 observations. *J. Geophys. Res.,* **101,** 7019–7032.

Mace, G. G., C. Jakob, and K. P. Moran, 1998: Validation of hydrometeor occurrence predicted by the ECMWF model using millimeter wave radar data. *Geophys. Res. Lett.,* **25,** 1645–1648.

Masunaga, H., and C. D. Kummerow, 2005: Combined radar and radiometer analysis of precipitation profiles for a parametric retrieval algorithm. *J. Atmos. Oceanic Technol.,* **22,** 909–929.

Matrosov, S. Y., T. Uttal, J. B. Snider, and R. A. Kropfli, 1992: Estimation of ice cloud parameters from ground-based infrared radiometer and radar measurements. *J. Geophys. Res.,* **97,** 20 675–20 683.

Miller, S. D., G. L. Stephens, C. K. Drummond, A. K. Heidinger, and P. T. Partain, 2000: A multisensor diagnostic satellite cloud property retrieval scheme. *J. Geophys. Res.,* **105,** 19 955–19 971.

Mitrescu, C., and G. L. Stephens, 2002: A new method for determining cloud transmittance and optical depth using the ARM micro-pulsed lidar. *J. Atmos. Oceanic Technol.,* **19,** 1073–1081.

Mugnai, A., E. A. Smith, and G. J. Tripoli, 1993: Foundations for statistical–physical precipitation retrieval from passive microwave satellite measurements. Part II: Emission-source and generalized weighting-function properties of a time-dependent cloud-radiation model. *J. Appl. Meteor.,* **32,** 17–39.

Nakajima, T., and M. D. King, 1990: Determination of the optical thickness and effective radius of clouds from reflected solar radiation measurements. Part I: Theory. *J. Atmos. Sci.,* **47,** 1878–1893.

Nakajima, T. Y., and T. Nakajima, 1995: Wide-area determination of cloud microphysical properties from NOAA AVHRR measurements for FIRE and ASTEX regions. *J. Atmos. Sci.,* **52,** 4043–4059.

Nesbitt, S. W., and E. J. Zipser, 2003: The diurnal cycle of rainfall and convective intensity according to three years of TRMM measurements. *J. Climate,* **16,** 1456–1475.

Ou, S. C., K.-N. Liou, W. M. Gooch, and Y. Takano, 1993: Remote sensing of cirrus cloud parameters using advanced very-high-resolution radiometer 3.7–10.9 μm channels. *Appl. Opt.,* **32,** 2171–2180.

Petty, G. W., 1999: Cloud physical and microwave radiative properties of tropical stratiform precipitation inferred from multichannel microwave radiances. Preprints, *10th Conf. on Satellite Meteorology and Oceanography,* Long Beach, CA, Amer. Meteor. Soc., 318–320.

Platnick, S., 2000: Vertical photon transport in cloud remote sensing problems. *J. Geophys. Res.,* **105,** 22 919–22 936.

——, and F. Valero, 1995: A validation study of a satellite cloud retrieval during ASTEX. *J. Atmos. Sci.,* **52,** 2985–3001.

——, R. Pincus, B. Wind, M. D. King, M. Gray, and P. Hubanks, 2004: An initial analysis of the pixel-level uncertainties in global MODIS cloud optical thickness and effective particle size retrievals. *Proc. SPIE,* **5652,** 30–40.

Platt, C. M. R., S. A. Young, P. J. Manson, G. R. Patterson, S. C. Marsden, R. T. Austin, and J. Churnside, 1998: The optical properties of equatorial cirrus from observations in the ARM pilot radiation observation experiment. *J. Atmos. Sci.,* **55,** 1977–1996.

Prabhakara, C., R. S. Fraser, G. Dalu, M.-L. C. Wu, R. J. Curran, and T. Styles, 1988: Thin cirrus clouds: Seasonal distribution over oceans deduced from Nimbus-4 IRIS. *J. Appl. Meteor.,* **27,** 379–399.

Robertson, F. R., D. E. Fitzgerald, and C. Kummerow, 2003: Effects of uncertainty in TRMM precipitation radar path integrated attenuation on interannual variations of tropical oceanic rainfall. *Geophys. Res. Lett.,* **30,** 1180–1183.

Rodgers, C. D., 1990: Characterization and error analysis of profiles retrieved from remote sounding measurements. *J. Geophys. Res.,* **95,** 5587–5595.

——, 2000: *Inverse Methods for Atmospheric Sounding: Theory and Practice.* World Scientific, 238 pp.

Rossow, W. B., and B. Cairns, 1995: Monitoring changes of clouds. *Climatic Change,* **31,** 305–347.

——, and R. A. Schiffer, 1999: Advances in understanding clouds from ISCCP. *Bull. Amer. Meteor. Soc.,* **80,** 2261–2288.

Sagan, C., and J. B. Pollack, 1967: Anisotropic nonconservative scattering and the clouds of Venus. *J. Geophys. Res.,* **72,** 469–477.

Salby, M., 1982: Sampling theory for asynoptic satellite observations. Part I: Spectra, resolution, and aliasing. *J. Atmos. Sci.,* **39,** 2577–2600.

——, and P. Callaghan, 1997: Sampling error in climate properties derived from satellite measurements: Consequences of undersampled diurnal variability. *J. Climate,* **10,** 18–36.

Skofronick-Jackson, G. M., J. R. Wang, G. M. Heymsfield, R. Hood, W. Manning, R. Meneghini, and J. A. Weinman, 2003: Combined radiometer–radar microphysical profile estimations with emphasis on high-frequency brightness temperature observations. *J. Appl. Meteor.,* **42,** 476–487.

——, M.-J. Kim, J. A. Weinamn, and D.-E. Chang, 2004: A physical model to determine snowfall over land by microwave radiometry. *IEEE Trans. Geosci. Remote Sens.,* **42,** 1047–1058.

Smith, E. A., and Coauthors, 1998: Results of WetNet PIP-2 project. *J. Atmos. Sci.,* **55,** 1483–1536.

——, A. Mehta, and J. M. Shepherd, 2002: Description of Global Precipitation Measurement (GPM) mission. NASA Goddard Space Flight Center, Tech. Memo., GPM Rep. Series 6, 25 pp.

Soden, B., and Coauthors, 2000: An intercomparison of radiation codes for retrieving upper-tropospheric humidity in the 6.3-mm band: A report from the first GVaP workshop. *Bull. Amer. Meteor. Soc.,* **81,** 797–808.

Spencer, R. W., H. M. Goodman, and R. E. Hood, 1989: Precipitation retrieval over land and ocean with the SSM/I: Identification and characteristics of the scattering signal. *J. Atmos. Oceanic Technol.,* **6,** 254–273.

Stephens, G. L., 1978: Radiation profiles in extended water clouds: II. Parameterization schemes. *J. Atmos. Sci.,* **35,** 2123–2132.

——, 1980: Radiative properties of cirrus clouds in the infrared region. *J. Atmos. Sci.,* **37,** 435–446.

——, 1994: *Remote Sensing of the Lower Atmosphere: An Introduction.* Oxford University Press, 523 pp.

——, 2005: Cloud feedbacks in the climate system: A critical review. *J. Climate,* **18,** 237–273.

——, R. Engelen, M. Vaughan, and T. L. Anderson, 2001: Toward retrieving properties of the tenuous atmosphere using space-based lidar measurements. *J. Geophys. Res.,* **106,** 28 143–28 157.

——, and Coauthors, 2002: The CloudSat mission and the A-Train. *Bull. Amer. Meteor. Soc.,* **83,** 1771–1790.

Stevens, B., and Coauthors, 2003: Dynamics and chemistry of marine stratocumulus—DYCOMS-II. *Bull. Amer. Meteor. Soc.,* **84,** 579–593.

Stevens, D. E., A. S. Ackerman, and C. S. Bretherton, 2002: Effects of domain size and numerical resolution of the simulations of shallow cumulus convection. *J. Atmos. Sci.,* **59,** 3285–3301.

Stone, R., G. L. Stephens, C. M. R. Platt, and S. Banks, 1990: The remote sensing of thin cirrus cloud using satellites, lidar and radiative transfer theory. *J. Appl. Meteor.,* **29,** 353–366.

Tao, W.-K., and J. Simpson, 1993: Goddard Cumulus Ensemble Model. Part I: Model description. *Terr. Atmos. Oceanic Sci.,* **4,** 35–72.

Twomey, S., and K. J. Seton, 1980: Inferences of gross microphysical properties of clouds from spectral reflectance measurements. *J. Atmos. Sci.,* **37,** 1065–1069.

van de Hulst, H. C., 1980a: *Multiple Light Scattering: Tables, Formulas, and Applications.* Vol. 1. Academic Press, 317 pp.

——, 1980b: *Multiple Light Scattering: Tables, Formulas, and Applications.* Vol. 2. Academic Press, 422 pp.

Wang, P.-H., P. Minnis, M. P. McCormick, G. S. Kent, and K. M. Skeens, 1996: A 6-year climatology of cloud occurrence frequency from Stratospheric Aerosol and Gas Experiment II observations (1985–1990). *J. Geophys. Res.,* **101,** 29 407–29 429.

Weng, F., T. Zhu, and B. Yan, 2007: Satellite data assimilation in numerical weather prediction models. Part II: Uses of rain-affected radiances from microwave observations for hurricane vortex analysis. *J. Atmos. Sci.,* **64,** 3910–3925.

Wielicki, B. A., and Coauthors, 1990: The 27–28 October 1986 FIRE IFO cirrus case study: Comparison of radiative transfer theory with observations by satellite and aircraft. *Mon. Wea. Rev.,* **118,** 2356–2376.

Wilheit, T., 1986: Some comments on passive microwave measurements of rain. *Bull. Amer. Meteor. Soc.,* **67,** 1221–1232.

——, and Coauthors, 1994: Algorithms for the retrieval of rainfall from passive microwave measurements. *Remote Sens. Rev.,* **11,** 163–194.

Wylie, D., D. L. Jackson, W. P. Menzel, and J. J. Bates, 2005: Trends in global cloud cover in two decades of HIRS observations. *J. Climate,* **18,** 3021–3031.

Yang, P., and K. Liou, 1998: Single scattering properties of complex ice crystals in terrestrial atmospheres. *Contrib. Atmos. Phys.,* **71,** 223–248.

Yeh, H., and K. Liou, 1983: Remote sounding of cloud parameters from a combination of infrared and microwave channels. *J. Climate Appl. Meteor.,* **22,** 201–203.